Research Square

Preprints are preliminary reports that have not undergone peer review.
They should not be considered conclusive, used to inform clinical practice,
or referenced by the media as validated information.

A conserved human population of TRAV26^{+} type II Natural Killer T cells solely recognise CD1d

Kean CY Poa
Infection and Immunity Program and Department of Biochemistry and Molecular Biology, Biomedicine Discovery Institute, Monash University, Clayton, Victoria 3800, Australia.

Christopher M Harpur
Department of Microbiology & Immunology, Peter Doherty Institute for Infection and Immunity, The University of Melbourne, Melbourne, Victoria 3010, Australia; Infection, Immunity and Global Health, Murdoch Children's Research Institute, Parkville, Victoria 3052, Australia.

Tan-Yun Cheng
Division of Rheumatology, Inflammation, and Immunity, Brigham and Women's Hospital and Harvard Medical School, Boston, MA 02115, United States.

Elena Batleska
Department of Microbiology & Immunology, Peter Doherty Institute for Infection and Immunity, The University of Melbourne, Melbourne, Victoria 3010, Australia; Infection, Immunity and Global Health, Murdoch Children's Research Institute, Parkville, Victoria 3052, Australia.

Catriona V Nguyen-Robertson
Department of Microbiology & Immunology, Peter Doherty Institute for Infection and Immunity, The University of Melbourne, Melbourne, Victoria 3010, Australia.

Rajesh Lamichhane
Department of Microbiology & Immunology, Peter Doherty Institute for Infection and Immunity, The University of Melbourne, Melbourne, Victoria 3010, Australia.

Caroline Soliman
Department of Microbiology & Immunology, Peter Doherty Institute for Infection and Immunity, The University of Melbourne, Melbourne, Victoria 3010, Australia.

Scott JJ Reddiex
Department of Microbiology & Immunology, Peter Doherty Institute for Infection and Immunity, The University of Melbourne, Melbourne, Victoria 3010, Australia.

Christopher Menne
Infection, Immunity and Global Health, Murdoch Children's Research Institute, Parkville, Victoria 3052, Australia. https://orcid.org/0000-0003-2211-8766

Adam P Uldrich
Department of Microbiology & Immunology, Peter Doherty Institute for Infection and Immunity, The University of Melbourne, Melbourne, Victoria 3010, Australia. https://orcid.org/0000-0002-6350-5976

D Branch Moody
Division of Rheumatology, Inflammation, and Immunity, Brigham and Women's Hospital and Harvard Medical School, Boston, MA 02115, United States.

Jamie Rossjohn
Infection and Immunity Program and Department of Biochemistry and Molecular Biology, Biomedicine Discovery Institute, Monash University, Clayton, Victoria 3800, Australia; Institute of Infection and Immunity, Cardiff University School of Medicine, Heath Park, Cardiff, CF14 4XN, United Kingdom.
https://orcid.org/0000-0002-2020-7522

Dale I Godfrey
Department of Microbiology & Immunology, Peter Doherty Institute for Infection and Immunity, The University of Melbourne, Melbourne, Victoria 3010, Australia. https://orcid.org/0000-0002-3009-5472

Daniel G Pellicci
Department of Microbiology & Immunology, Peter Doherty Institute for Infection and Immunity, The University of Melbourne, Melbourne, Victoria 3010, Australia; Infection, Immunity and Global Health, Murdoch Children's Research Institute, Parkville, Victoria 3052, Australia; Department of Paediatrics, The University of Melbourne, Melbourne, Victoria 3010, Australia https://orcid.org/0000-0001-5305-2398

Jérôme Le Nours
Infection and Immunity Program and Department of Biochemistry and Molecular Biology, Biomedicine Discovery Institute, Monash University, Clayton, Victoria 3800, Australia.

Catarina F Almeida
catarina.dos@unimelb.edu.au

Department of Microbiology & Immunology, Peter Doherty Institute for Infection and Immunity, The University of Melbourne, Melbourne, Victoria 3010, Australia. https://orcid.org/0000-0002-3393-4411

Article

Keywords:

Posted Date: December 5th, 2025

DOI: https://doi.org/10.21203/rs.3.rs-7004764/v1

License: This work is licensed under a Creative Commons Attribution 4.0 International License. Read Full License

Additional Declarations: Yes there is potential Competing Interest. D. I. G and C. F. A hold two patents on CD1-targetting for immune modulation.

Version of Record: A version of this preprint was published at Nature Communications on October 7th, 2026. See the published version at https://doi.org/10.1038/s41467-026-78124-5.

Abstract

Most studies of CD1d-restricted Natural killer T cells (NKT) have focussed on type I *TRAV10-TRAJ18*$^{+}$ NKT cells that recognise the glycolipid a-GalCer. Our understanding of type II NKT cells, their TCR gene usage and ligand diversity remains unclear. Here, using CD1d tetramers carrying diverse endogenous lipids (CD1d-endo), we identified public human TRAV26^{+} type II NKT TCRs present in all individuals, with many expressing a conserved *TRAV26-2-TRAJ48* TCRa chain. Cellular, molecular and lipidomic analyses showed that TRAV26^{+} TCRs bound with similar affinities to CD1d loaded with diverse lipids, suggesting lipid-independent binding. Crystal structures of TRAV26^{+} TCR-CD1d complexes showed these TCRs bound solely to the A'-roof of CD1d, distant from the protruding lipid. Collectively we have uncovered a population of public lipid-independent TRAV26^{+} type II NKT cells, suggesting a potential role in diseases where aberrant CD1d expression occurs.

INTRODUCTION

Natural Killer T (NKT) cells recognise lipid-based antigens (Ags) presented by the monomorphic MHC class I-like molecule CD1d. NKT cells are generally classified into two main groups, type I and II NKT cells [1]. Most studies have focussed on type I NKT cells, which express an evolutionary conserved public T cell receptor (TCR) repertoire in humans, defined by an invariant *TRAV10-TRAJ18*$^{+}$ TCRα chain paired with *TRBV25-1*$^{+}$ TCRβ chains, that confers co-recognition of a prototypical glycolipid Ag known as α-galactosylceramide (α-GalCer) and related hexosyl ceramides when bound to CD1d [2, 3]. The use of CD1d-α-GalCer tetramers has enabled extensive research to characterise the phenotypic profile and function of type I NKT cells [1, 2].

Type II NKT cells were identified circa 30 years ago in mice as CD4^{+} T cells that do not recognize MHC class II [4, 5], or as CD1d-reactive cells that do not require CD1d recycling to endosomes[6]. Those studies suggested that type II NKT cells express diverse TCR genes, distinct from the semi-invariant TCR characteristic of type I NKT cells, and are therefore commonly described as 'diverse' NKT cells [1]. In contrast to type I NKT cells, type II NKT cells do not recognize α-GalCer but can be activated by other CD1d-bound lipid-based Ags including sulfatides and phospholipids as well as small molecules [2, 5, 7]. Type II NKT cells appear to play a unique role in the immune system [2], with some studies in humans suggesting opposing roles to type I NKT cells [8, 9]. Type II NKT cells are comprised of specialized subsets capable of monitoring biological processes that impact on lipid metabolism and consequently, on the self-lipids bound to CD1d [5, 10, 11, 12, 13]. These cells are associated with, or implicated in, various diseases such as hepatitis, ulcerative colitis, and cancer [8, 9]. In humans, type II NKT cells appear to outnumber type I NKT cells [14, 15, 16]. However, the paucity of reagents to clearly identify type II NKT cells has left fundamental questions unanswered that include the identity of immunodominant Ags, TCR patterns, the underlying mechanisms that regulate their numbers and the molecular mechanism of Ags recognition [2].

Insights have been gained into the molecular mechanism that underpins the recognition of CD1d-lipid complexes by human and mouse type I NKT TCRs [17, 18] as well as mouse type II NKT TCRs [19, 20, 21] and 'atypical' NKT cells [22, 23, 24, 25, 26]. These studies led to the fundamental principle that underscored the NKT TCR co-recognition paradigm of CD1d-lipid complexes whereby the NKT TCR contacted both CD1d and the presented Ag[3]. However, our understanding of the molecular mechanism that underpins the recognition of CD1d-lipid by human type II NKT TCRs remains less clear.

Here, using human CD1d tetramers presenting endogenous lipids, we identify a population of public type II NKT cells that express a TRAV26^{+} TCRa chain. Lipidomic scanning of Ags contained within CD1d-TRAV26^{+} TCR complexes revealed a diverse array of lipids, and structural determination of the ternary complex showed that the TCR contacted CD1d in an Ag-independent manner.

RESULTS

Identification of human CD1d-endo-reactive NKT cells.

Early studies suggested that type II NKT cells can recognise and respond to CD1d carrying endogenous lipids (CD1d-endo) [4, 6, 14, 15, 16, 27, 28]. Although some target lipid-Ags for type II NKT cells are known, the study of these cells has been hindered by a limited understanding of their target lipid repertoire. To further investigate the antigenic targets and diversity of human type II NKT cells, CD1d-endo tetramers were generated using glycosylation-deficient GnTI$^{-/-}$ Human Embryonic Kidney 293 (HEK293S) cells to express soluble CD1d ectodomains that incorporate a cellular cargo of endogenous lipids during synthesis [29, 30]. These CD1d-endo tetramers stained over 0.1% of live CD3^{+} T cells within peripheral blood mononuclear cells (PBMCs) from healthy human donors, albeit with varied and often low mean fluorescence intensity (MFI) in many cases (Fig. 1a and S1a). After one round of tetramer-associated magnetic enrichment (TAME) [31] using phycoerythrin (PE)-labelled CD1d-endo tetramers, the frequency of the CD1d-endo tetramer^{+} amongst CD3^{+} T cells generally yielded more defined populations at proportions ranging up to 13% (Median (M) 0.92%, interquartile range (IQR) 0.3–1.9%), in contrast to PE-conjugated streptavidin (SAV-PE) negative controls where no clear population was identified (**Fig. S1a**). However, it was possible that some of these frequencies may be impacted by non-TCR CD1d ligands such as CD36 family members [32], as suggested by the enrichment of CD3^{-} cells capturing the CD1d-tetramer after TAME (Fig. 1a and S1a-b). To minimise this, for many samples, we used a CD42b exclusion gate to exclude platelets which express high levels of CD36 and/or CD36 blocking antibody prior to staining of some samples.

To confirm TCR-dependent CD1d-binding specificity, CD3^{+} CD1d-endo tetramer^{+} cells were enriched using flow cytometric cell sorting and expanded in culture for 18–20 days and re-stained with CD1d-endo tetramers. The CD1d-endo tetramer^{+} populations varied widely in frequency (0.035-100%) of CD3^{+} cells (Fig. 1a) but often formed more distinct clusters (M = 0.84%, IQR = 0.2–8.4%), when compared to post-MACS enriched samples. This may be because the expanded cells were devoid of platelets or other cell types that, through cell adhesion and/or trogocytosis, may confer TCR-independent binding with CD1d-tetramers (Fig. 1 and S1a) [32]. CD1d-endo tetramer^{+} cells included both αβ and γδ T cells, with γδ T cell frequencies varying widely in the 25 donors

analysed. CD1d-endo-tetramer^{+} αβ T cells in these cultures (Fig. 1b) were skewed towards CD4^{+} single positive (SP) expression (M 80%, IQR 46–94%), although CD8^{+} SP and CD4^{-}CD8^{-} double negative (DN) populations were also detected at lower frequencies (Fig. 1c). Conversely, the CD1d-endo tetramer^{-} conventional T cells had similar frequencies of CD4^{+} SP and CD8^{+} SP T cells.

By co-labelling expanded cells with CD1d-endo tetramer and CD1d-α-GalCer tetramer, many CD1d-binding cells (M 80%, IQR 39–95%) co-stained with both tetramers (Fig. 1d). In the three donors shown, representative of 18 analysed this way, the staining pattern revealed distinct T cell clusters that likely reflected the oligoclonality of expanded NKT cells. Most, but not all, clusters showed a positive correlation for staining intensity by both tetramers, suggesting that binding to CD1d occurs regardless of the lipids within the CD1d cleft.

The functional potential of expanded cells was also investigated. After stimulation with phorbol 12-myristate 13-acetate (PMA) and ionomycin, CD1d-endo tetramer^{+} cells expressed tumour necrosis factor (TNF) and interferon-g (IFNg) (mean 66% and 26%, respectively (Fig. 1e), and cytokine production was detected in both CD8^{-} and CD8^{+} cells (**Fig. S1c**). While some CD1d-endo tetramer^{+} cells co-produced these cytokines (mean 20%), some produced either one or the other (Fig. 1e). IL-13 was only detected in a small subset of CD1d-endo tetramer^{+} cells in some donors, in contrast to CD1d-endo tetramer^{-} cells where IL-13 was more frequently detected (Fig. 1e). Thus, type II NKT cell populations capable of producing pro-inflammatory cytokines are readily identified among human donors by CD1d-endo tetramers with no defined exogenously loaded antigen.

TRAV26 TCR bias amongst human CD1d-endo-reactive T cells.

To characterise the TCR repertoire of the populations labelled by CD1d-endo tetramers, single CD1d-endo tetramer^{+} cells were index sorted from *in vitro* expanded cultures and their TCR sequences were determined [31]. Paired TCRα and TCRβ, or TCRδ and TCRγ chain-transcripts were determined for cells sorted as αβ T cells or γδ T cells (Tables 1 and 2). None of the sorted T cell clones contained the canonical TCR usage that define type I NKT TCRs. Instead, they exhibited a varied, yet biased, range of γδ and αβ TCR chains (Fig. 2a-b **and** Tables 1 and 2). Almost all γδ TCRs analysed incorporated *TRDV1* genes (17 of 18 Vδ sequences derived from 11 donors (Table 1), in line with previous studies that described Vd1^{+} γδ T cells recognizing CD1d [22, 23, 33] and CD1c [34]. Unexpectedly, within the αβ TCRs, there was a strong bias towards TRAV26^{+} TCRs, with ~ 65% of αβ TCRs within CD1d-endo tetramer^{+} cells from 11 donors utilising *TRAV26*-2 gene segments. In addition, cells from 5 donors also utilised *TRAV26-1*, which differs from *TRAV26-2* by four germline encoded amino acids, as well as one amino acid in the CDR3α loop (Fig. 2a **and** Table 2). Further, *TRAV26-2 gene* segments were often associated with *TRAJ48* in 17 of 39 TCRs (Fig. 2a **and** Table 2), although other TRAJ gene-rearrangements were also detected, including *TRAJ42* in 6 of 39 TCRs, *TRAJ23* in 5 of 39 TCRs and *TRAJ45* in 4 of 39 TCRs (Fig. 2a **and** Table 2). Type II NKT cells possessing *TRAJ48* genes almost exclusively rearranged with *TRAV26*$^{+}$, with 17 encoded by *TRAV26-2* and one by *TRAV26-1*. Moreover, a conserved CDR3α involving the insertion of the same amino acid (G in position 6) in the N-region during rearrangements between *TRAV26-2* and *TRAJ48* genes was identified in 5 donors across 5 independent experiments (Fig. 2b **and** Table 2), demonstrating public conservation of the CDR3a sequence. Notably, this same *TRAV26-2–TRAJ48* rearrangement had also been reported in a single NKT cell clone isolated *via* a different approach [25]. Another conserved motif was detected in positions 6 and 7 of the TRAV26-2 CDR3a sequences, where proline was also often seen at position 6, typically accompanied by bulky residue at position 7 (Fig. 2b **and** Table 2). In contrast to the conserved TCRα chain, the TCRβ gene usage was highly diverse, as were the CDR3β sequences and lengths (Table 2).

Table 1

Paired gd TCR sequences of CD1d-endo tetramer + single-sorted cells IMGT TCR gene nomenclatures and associated complementary determining region tetramers post-sort/expansion in culture for 21 d as per Fig. 1a. The number of observations (obs. column) as well as intra-donor frequency at which each ur analysis of 11 donors. A total of three sorting experiments were performed. Red residues are either partially or fully non-germline encoded. XX means undet given a clone name. Amino acid positions: CDR1-IMGT (27 to 38), CDR2-IMGT (56 to 65), and

Clone	Donor	TRDV	TRDJ	TRDD	CDR1d	CDR2d	CDR3d (non germline)			TRGV	TRGJ
VD3G8	C4	TRDV3*01	TRDJ2*01	TRDD3*01	TVYS…NPD	GDN…SRS	CAF	RGTGGYPWA	AQLFF	TRGV8*01	TRGJ2
	C3	TRDV1*01	TRDJ1*01	TRDD2*01	TSWW…SYY	QG…S	CALGE	LLYPI	TDKLIF	-	
	C1	TRDV1*01	TRDJ1*01	TRDD3*01	TSWW…SYY	QG…S	CALGE	LRVGWGR	LIF	TRGV5*01	TRGJ1
	CA1	TRDV1*01	TRDJ1*01	TRDD3*01	TSWW…SYY	QG…S	CALGE	LAFFT	TDKLIF	TRGV8*01	TRGJ1
	CA2	TRDV1*01	TRDJ1*01	TRDD3*01	TSWW…SYY	QG…S	CALGE	SGIRLY	TDKLIF	TRGV8*01	TRGJP
	CA3	TRDV1*01	TRDJ1*01	TRDD3*01	TSWW…SYY	QG…S	CALGE	QVVYWGIRTM	TDKLIF	TRGV5*01	TRGJP
	CA3	TRDV1*01	TRDJ1*01	TRDD3*01	TSWW…SYY	QG…S	CALGE	LPGGYAG	LIF	TRGV4*01	TRGJ1
	CA4	TRDV1*01	TRDJ1*01	TRDD2/TRDD3*01	TSWW…SYY	QG…S	CALG	DPASYPFVLGD	TDKLIF	TRGV5*01	TRGJP
	CA4	TRDV1*01	TRDJ1*01	TRDD2/TRDD3	TSWW…SYY	QG…S	CALG	DPASYPFVLGD	TDKLIF	-	
	G58	TRDV1*01	TRDJ1*01	TRDD3*01	TSWW…SYY	QG…S	CALGE	SRTGGYARG	KLIF	TRGV4*01	TRGJ1 TRGJ2
	G58	TRDV1*01	TRDJ1*01	TRDD3*01	TSWW…SYY	QG…S	CALG	DSRRDKAY	TDKLIF	TRGV5*01	TRGJ1 TRGJ2
	G59	TRDV1*01	TRDJ1*01	TRDD3*01	TSWW…SYY	QG…S	CALG	DPGVTH	TDKLIF	TRGV3*01	TRGJ1 TRGJ2
	G59	TRDV1*01	TRDJ1*01	TRDD3*01	TSWW…SYY	QG…S	CALGE	RRIRGVN	TDKLIF	TRGV2*01	TRGJ1 TRGJ2
	G60	TRDV1*01	TRDJ1*01	TRDD3*01	TSWW…SYY	QG…S	CALGE	NGYWG	TDKLIF	TRGV3*01	TRGJ1 TRGJ2
	G60	TRDV1*01	TRDJ2*01	TRDD3*01	TSWW…SYY	QG…S	CALGE	LRVLGA	LTAQLFF	TRGV4*01	TRGJ1 TRGJ2
	G62	TRDV1*01	TRDJ1*01	TRDD3*01	TSWW…SYY	QG…S	CALGE	TSYGGTGGYGVD	TDKLIF	-	
	G62	TRDV1*01	TRDJ1*01	TRDD2*01	TSWW…SYY	QG…S	CALGE	RYLPTA	DKLIF	TRGV9*01	TRGJ1 TRGJ2
	G62	TRDV1*01	TRDJ1*01	TRDD3*01	TSWW…SYY	QG…S	CALG	GLIYKGDSASLGG	TDKLIF	-	

Table 2

Paired ab TCR sequences of CD1d-endo tetramer + single-sorted cells IMGT TCR gene nomenclatures and associated complementary determining regior tetramers post-sort/expansion in culture for 21 d as per Fig. 1a. The number of observations (obs. column) as well as intra-donor frequency at which each u analysis of 14 donors. Sequences in bold contain the invariant TRAV26-TRAJ48 rearrangement. A total of eight single-cell sorting experiments were performe to generate αβ NKT cell clones are given a clone name. Amino acid positions: CDR1-IMGT (27 to 38), CDR2-IM

Clone	Donor	TRAV	TRAJ	CDR1a	CDR2a	CDR3a (non germline)			TRBV	TRBJ	TRBD
iT26	**4A**	**TRAV26-2*01**	**TRAJ48*01**	**TISG…TDY**	**GLT…SN**	**CILRD**	**G**	**FGNEKLTF**	**TRBV6-2*01**	**TRBJ2-1*01**	**TRBD1**
	4A	TRAV26-1*01	TRAJ44*01	TISG…NEY	GLK…NN	CIVR	ASWR	TGTASKLTF	-		
	4A	TRAV4*01	TRAJ13*01	NIAT…NDY	GYK…TK	CL	GPL	NSGGYQKVTF	TRBV28-1*01	TRBJ1-1*01	TRBD1
	4A	TRAV13-1*01 or TRAV13-2*01	TRAJ9*01	DSA…SNY	IRSN…VGE	CA	VS	NTGGFKTIF	TRBV5-5*01	TRBJ1-1*01	TRBD1
				NSA…SDY	IRSN…MDK	CA					
	4A	TRAV8-2*01	TRAJ49*01	SSY…SPS	YTSA…ATLV	CVVS	GG	TGNQFYF	TRBV4-1*01	TRBJ2-1*01	TRBD2
	4A	TRAV27*01	TRAJ23*01	SVF…SS	VVTG…GEV	CAG	VS	IYNQGGKLIF	TRBV4-2*01	TRBJ2-1*01	TRBD1
	4G	TRAV26-2*01	TRAJ48*01	TISG…TDY	GLT…SN	CIL	SSG	FGNEKLTF	TRBV4-1*01	TRBJ2-5	TRBD2
	4G	**TRAV26-2*01**	**TRAJ48*01**	**TISG…TDY**	**GLT…SN**	**CILRD**	**G**	**FGNEKLTF**	**TRBV5-6*01**	**TRBJ2-6*01**	**TRBD1**
	4G	TRAV26-2*01	TRAJ42*01	TISG…TDY	GLT…SN	CILRD	GFM	NYGGSQGNLIF	TRBV19*01	TRBJ1-5*01	TRBD2
	4G	TRAV26-2*01	TRAJ48*01	TISG…TDY	GLT…SN	CILR	APF	NFGNEKLTF	TRBV28*01	TRBJ1-2*01	TRBD2
	4G	TRAV26-2*01	TRAJ42*01	TISG…TDY	GLT…SN	CILR	F	NYGGSQGNLIF	-		
	4G	TRAV26-2*01	TRAJ45*01	TISG…TDY	GLT…SN	CILRD	GFSV	YSGGGADGLTF	-		
	4K	TRAV26-1*01	TRAJ48*01	TISG…NEY	GLK…NN	CIVRV	VV	FGNEKLTF	TRBV6-1*01	TRBJ1-2*01	TRBD1
	C3	TRAV26-1*01	TRAJ41*01	TISG…NEY	GLK…NN	CI	G	NSGYALNF	TRBV6-2*01	TRBJ2-7*01	TRBD2
	C3	TRAV26-2*01	TRAJ48*01	TISG…TDY	GLT…SN	CIL	GAPY	NFGNEKLTF	TRBV6-5*01	TRBJ2-7*01	TRBD1
	C3	TRAV26-2*01	TRAJ23*01	TISG…TDY	GLT…SN	CILRD	GFE	IYNQGGKLIF	TRBV20-1*01	TRBJ2-6*01	TRBD1
	C3	TRAV26-2*01	TRAJ48*01	TISG…TDY	GLT…SN	CILR	PGF	FGNEKLTF	TRBV7-2*01	TRBJ2-5*01	TRBD2
	C3	TRAV26-2*01	TRAJ48*01	TISG…TDY	GLT…SN	CI	NQVY	NFGNEKLTF	TRBV12-4*01	TRBJ2-2*01	TRBD1
	C3	TRAV10*01	TRAJ17*01	VSP…FSN	MTFS…ENT	CVVS	AG	AAGNKLTF	TRBV4-1*01	TRBJ2-4*01	TRBD2
	C3	TRAV29/DV5*01	TRAJ54*01	NSM…FDY	ISSI…KDK	CAAS	PI	IQGAQKLVF	-		
	C4	TRAV26-2*01	TRAJ32*01	TISG…TDY	GLT…SN	CILRD	FGG	NYGGATNKLIF	TRBV27*01	TRBJ2-2	UNCLE
T26B	C4	TRAV26-2*01	TRAJ42*01	TISG…TDY	GLT…SN	CILRD	GFK	NYGGSQGNLIF	TRBV13-1*01	TRBJ2-7*01	TRBD2
T26A	C4	TRAV26-2*01	TRAJ40*01	TISG…TDY	GLT…SN	CILRD	GWG	GTYKYIF	TRBV19-1*01	TRBJ2-7*01	TRBD1
	C4	TRAV26-2*01	TRAJ29*01	TISG…TDY	GLT…SN	CILRD	GW	SGNTPLVF	-		
	C4	TRAV26-2*01	TRAJ48*01	TISG…TDY	GLT…SN	CILR		NFGNEKLTF	TRBV24-1*01	TRBJ1-1*01	TRBD1

Clone	Donor	TRAV	TRAJ	CDR1a	CDR2a	CDR3a (non germline)			TRBV	TRBJ	TRBD
	CA1	TRAV26-2*01	TRAJ42*01	TISG…TDY	GLT…SN	CILRD	GFE	NYGGSQGNLIF	TRBV20-1*01	TRBJ1-2*01	TRBD2
	CA1	TRAV26-2*01	TRAJ23*01	TISG…TDY	GLT…SN	CILRD	GFM	IYNQGGKLIF	-		
	CA1	TRAV26-2*01	TRAJ36*01	TISG…TDY	GLT…SN	CILR	NPL	TGANNLFF	TRBV30*01	TRBJ1-6*01	TRBD1
	CA1	TRAV26-2*01	TRAJ54*01	TISG…TDY	GLT…SN	CILRD	GFGKF	QGAQKLVF	-		
	CA2	TRAV26-2*01	TRAJ42*01	TISG…TDY	GLT…SN	CILRD	GWA	NYGGSQGNLIF	-		
	CA3	TRAV26-2*01	TRAJ30*01	TISG…TDY	GLT…SN	CILRD	PL	DDKIIF	-		
	CA3	TRAV29/DV5*01	TRAJ48*01	NSM…FDY	ISSI…KDK	CAAS	PTIS	NFGNEKLTF	-		
	CA4	TRAV14/DV4*01	TRAJ43*01	TSDQ…SYG	QGSY…DEQN	CAMRE	G	NNDMRF	TRBV2*01	TRBJ2-7*01	TRBD2
	CA4	TRAV38-2/DV8*01	TRAJ33*01	TSES…DYY	QEAY…KQQN	CA	M	DSNYQLIW	TRBV24-1*01	TRBJ2-1*01	TRBD2
	CA4	TRAV35*01	TRAJ34*01	SIF…NT	LYKA…GEL	CA	ST	SYNTDKLIF	TRBV28*01	TRBJ2-5*01	TRBD1
	CA4	TRAV38-2/DV8*01	TRAJ52*01	TSES…DYY	QEAY…KQQN	CA	YP	NAGGTSYGKLTF	-		
	CH5	TRAV26-2*01	TRAJ48*01	TISG…TDY	GLT…SN	CIL	QAPFN	FGNEKLTF	TRBV10-3	TRBJ1-1*01	TRBD2
	CH5	TRAV26-2*01	TRAJ48*01	TISG…TDY	GLT…SN	CILR	APL	NFGNEKLTF	TRBV19*01	TRBJ2-2*01	TRBD1
	CH5	**TRAV26-2*01**	**TRAJ48*01**	**TISG…TDY**	**GLT…SN**	**CIRLD**	**G**	**FGNEKLTF**	**TRBV19*01**	**TRBJ2-7**	**TRBD1**
	CH5	TRAV26-2*01	TRAJ34*01	TISG…TDY	GLT…SN	CILRD	PWD	TDLKIF	TRBV3-1	TRBJ2-2*01	TRBD1
	CH5	TRAV29*01	TRAJ26*01	NSM…FDY	ISSI…KDK	CAAS	EILK	GQNFVF	TRBV20-1*01	TRBJ2-1*01	TRBD2
	CH5	TRAV17*01	TRAJ11*01	TSI…NN	IRSN…ERE	CATD	TT	GYSTLTF	TRBV4-2*01		
	CH5	TRAV26-1*01	TRAJ37*01	TISG…NEY	GLK…NN	CIVRV	F	NTGKLIF	-	TRBJ2-7*01	TRBD2
	CH7	TRAV26-1*01	TRAJ20*01	TISG…NEY	GLK…NN	CIVRV	APPF	NDYKLSF	TRBV6-1*01		
	CH7	TRAV26-2*01	TRAJ43*01	TISG…TDY	GLT…SN	CILRD	GFGL	NNDMRF	TRBV10-2*01	TRBJ1-1*01	TRBD1
	CH7	TRAV26-2*01	TRAJ23*01	TISG…TDY	GLT…SN	CILRD	PL	IYNQGGKLIF	TRBV14*01/*02	TRBJ2-7*01	TRBD1
	CH7	TRAV26-2*01	TRAJ45*01	TISG…TDY	GLT…SN	CILRD	GFRVY	YSGGGADGLTF	TRBV9*02	TRBJ2-3*01	TRBD1
	CH7	TRAV26-2*01	TRAJ48*01	TISG…TDY	GLT…SN	CIL	GAPG	FGNEKLTF	-	TRBJ2-3*01	TRBD1
	CH7	TRAV26-2*01	TRAJ23*01	TISG…TDY	GLT…SN	CILRD	PL	IYNQGGKLIF	-		
	CH8	**TRAV26-2*01**	**TRAJ48*01**	**TISG…TDY**	**GLT…SN**	**CILRD**	**G**	**FGNEKLTF**	**TRBV27*01**		
	CH8	TRAV26-2*01	TRAJ57*01	TISG…TDY	GLT…SN	CILRD	GWGLV	TQGGSEKLVF	TRBV9*01	**TRBJ1-1*01**	**TRBD1**
	CH8	TRAV26-2*01	TRAJ42*01	TISG…TDY	GLT…SN	CILRD	GFS	NYGGSQGNLIF	TRBV27*01	TRBJ1-1*01	TRBD1
	CH8	TRAV41*01	TRAJ49*01	VGI…SA	LSS…GK	CAV	PSV	GNQFYF	-	TRBJ2-7*01	TRBD2

Clone	Donor	TRAV	TRAJ	CDR1a	CDR2a	CDR3a (non germline)			TRBV	TRBJ	TRBD
	MSC3	TRAV14/DV4*01	TRAJ49*01	TSDQ…SYG	QGSY…DEQN	CAMRE	GYL	NTGNQFYF	TRBV24-1*01		
	MSC4	TRAV26-2*01	TRAJ45*01	TISG…TDY	GLT…SN	CILRD	GFLM	YSGGGADGLTF	TRBV3-1*01	TRBJ2-1*01	TRBD1*
	MSC4	TRAV26-2*01	TRAJ45*01	TISG…TDY	GLT…SN	CILRD	GWGM	YSGGGADGLTF	TRBV20-1*01	TRBJ2-3*01	TRBD1*
	MSC4	TRAV41*01	TRAJ45*01	VGI…SA	LSS…GK	CAV	T	SGGGADGLTF	TRBV4-1*01	TRBJ2-1*01	TRBD2*
	MSC4	TRAV26-2*01	TRAJ40*01	TISG…TDY	GLT…SN	CILRD	GWG	GTYKYIF	-	TRBJ1-1*01	TRBD1*
	MSC4	TRAV14/DV4*01	TRAJ27*01	TSDQ…SYG	QGSY…DEQN	CAMR		NTNAGKSTF	-		
	MSC4	TRAV26-2*01	TRAJ48*01	TISG…TDY	GLT…SN	CILR	APFR	FGNEKLTF	-		
	MSC4	**TRAV26-2*01**	**TRAJ48*01**	**TISG…TDY**	**GLT…SN**	**CILRD**	**G**	**FGNEKLTF**	-		

Single-cell index-sorting analysis of TCR gene expression revealed that the subpopulations co-staining with both CD1d-endo and CD1d-α-GalCer tetramers mainly comprised TRAV26$^+$ TCRs, indicated by red dots in the two representative donors (Fig. 2c). These cells were also CD4$^+$ (M = 100%) in 5 out of 6 donors analysed over 5 different index-sorting experiments, while in one donor, they were CD4$^-$CD8$^-$DN or CD4$^-$CD8^{low} (Fig. 2c). In summary, the human CD1d-endo-reactive population harbours a public type II NKT repertoire characterised by biased *TRAV26$^+$* TCR usage and a semi-conserved CDR3a motif, often expressed as a canonical *TRAV26-2-TRAJ48* rearrangement.

TRAV26$^+$ TCRs directly recognise CD1d.

To test the specificity of the CD1d-endo-reactive TCRs, five paired TCRs that included three TRAV26$^+$ clones ("T26A", *TRAV26-2-TRAJ40 TRBV19*, "T26B" *TRAV26-2-TRAJ42 TRBV13-1* and "iT26", *TRAV26-2-TRAJ48 TRBV6-2*), and two TRAV26$^-$ clones (an αβ TCR identified in [7], "T14", *TRAV14-TRAJ34 TRBV19*, and a γδ TCR "VD3G8", *TRDV3-TRDJ2 TRG8*) (Tables 1 and 2) were transiently transfected into HEK293T cells, or transduced β2m-deficient SKW3 cells (SKW3.β2m$^{-/-}$). These two TCR transduced cell systems were assessed for binding CD1d-α-GalCer and CD1d-endo tetramers, in comparison to a control cell line expressing a type I NKT TCR "NKT15" [35], or non-NKT controls including the T29_E [7] and the CD1c-reactive clone 3C4 [32] (Fig. 2d). The five lines stained strongly with CD1d-endo tetramers, with MFIs > 45000 in HEK293T or > 1000 in SKW3.β2m$^{-/-}$ cells (Fig. 2d), unlike the negative controls. While CD1d-α-GalCer tetramers showed much lower staining of the TRAV26– lines (typically 10-100-fold less than CD1d-endo), they stained all three TRAV26$^+$ lines to a similar degree as CD1d-endo tetramers (Fig. 2d), reflecting the co-staining profile observed after *in vitro* expansion of the parental clones (Fig. 2c). This suggested that the TRAV26$^-$ TCRs may detect an undefined mammalian endogenous lipid presented by CD1d, and that a-GalCer can displace this lipid thereby preventing recognition, whereas the TRAV26$^+$ lines are indifferent to the presence of a-GalCer. As expected, the type I NKT15 TCR line stained far more strongly with CD1d-α-GalCer tetramers (Fig. 2d), whereas the CD1d-restricted lines were not stained by SAV-PE alone, nor by CD1c-tetramers conjugated to PE (Fig. 2d), which instead specifically stained the 3C4 control.

To measure TCR-mediated activation following CD1d binding, NKT TCR-transduced cell lines were co-cultured with Ag-presenting cells with differing levels of CD1d. These included: wildtype C1R cells (C1R.WT) with low CD1d expression, CD1d transductants (C1R.CD1d) with high CD1d expression, or β2m knockout C1R cells (C1R.β2m$^{-/-}$) that lack surface CD1d [7]. The TCR-transduced lines derived from CD1d-endo sorted cells upregulated the activation marker CD69 when co-cultured with C1R.CD1d, whereas C1R.WT or C1R C1R.β2m$^{-/-}$ cells did not cause activation (Fig. 2e). α-GalCer elicited strong responses by the NKT15 cell line using C1R.WT or C1R.CD1d, whereas similar activation was observed in the presence or absence of α-GalCer for TRAV26$^-$ or TRAV26$^+$ lines (Fig. 2e). Notably, α-GalCer did not block activation of the TRAV26$^-$ lines despite blocking CD1d tetramer staining of these lines (Fig. 2d), suggesting that a-GalCer was unable to saturate all CD1d molecules on the C1R Ag-presenting cells in these co-culture conditions. Thus, the newly identified TCRs confer signalling in response to CD1d, regardless of whether α-GalCer is present. Taken together, these data suggest that TRAV26$^+$ NKT cells bind CD1d in a lipid-independent manner and represent a distinct population of human type II NKT cells.

Trapping lipids between CD1d and TCRs.

Two hypotheses regarding the role of lipids in CD1d-TCR binding were investigated. The first was that TRAV26$^+$ TCRs bind CD1d in a lipid-independent fashion, reminiscent of what has been reported for CD1a [36, 37] and CD1c [38]. The second, supported by studies of known type II NKT cell ligands, sulfatides [39] and membrane phospholipids [40], was that some as yet unknown but ubiquitous self-lipid can increase the TCR binding-affinity to CD1d and that a-GalCer can substitute for this lipid. To test these hypotheses, the 'TCR trap' method [41, 42] was employed whereby the soluble TCRs were allowed to form a complex with CD1d-endo that was subsequently purified using size exclusion chromatography, where TCR-bound CD1d molecules can be separated from non-bound CD1d molecules (Fig. 3a). The eluents of CD1d-TCR were then compared to CD1d alone by mass spectrometry analysis to identify the lipids specifically associated with CD1d-TCR binding.

The human CD1d-endo carries a heterogenous cargo of self-lipids that are detectable by nano-electrospray and reversed phase high performance liquid chromatography-mass spectrometry (Fig. 3a) [41, 42]. Nano-electrospray analysis was conducted on lipids that were eluted from the TCR alone, CD1d alone and CD1d in complex with the two TRAV26$^+$ αβ TCRs (T26A and T26B), the γδ TCR (VD3G8) and the TRAV26$^-$ αβ TCR (T14) (Fig. 3b). For TCR alone no clear signals for lipid binding were observed, as expected (Fig. 3a). In contrast, for CD1d alone, there were many *m/z* signals in negative mode. Similar to recent results with CD1a [37], and other CD1 molecules [30] the strongest signals matched the absolute mass and alkane series patterns for sphingomyelins (SM, *m/z* 737.6, 765.6, 819.6, 845.6 and 847.6) and some weak signals matched for phosphatidylcholine (PC, *m/z* 794.6, 904.7, 906.7, 932.7 and 934.7), which are the two most abundant cellular sphingolipid and phospholipid classes, respectively. In contrast to results from a type I NKT TCR-trap study in which the TCR strongly influenced the lipids bound to CD1d [42], CD1d in complex with T26A, T26B, VD3G8 and T14 showed a lipid pattern that was highly similar to CD1d alone. Using HPLC-MS as a more quantitative method that separates individual molecules for detection in very narrow mass windows, once again the distinct nature of each TCR in the four types of CD1d-TCR complexes, did not substantially affect the repertoire of lipids that mediated its binding to CD1d [42]. Indeed, in all cases, the patterns of lipids in CD1d-TCR complexes matched the patterns of lipids seen for CD1d endo alone (Figs. 3a and 3b), maintaining high SM to PC ratio [30]. Thus, no particular exogenous lipid was required for CD1d-TRAV26$^+$ TCR complex formation, supportive of the first hypothesis that these TCRs bind in Ag-independent manner.

To independently assess reactivity towards individual lipid species that include known CD1d-presented Ags that might be under-represented or absent from the mixed cargo of endogenous lipids, (dominated by SMs and PCs that were incorporated into CD1d during its biosynthesis in GnTI$^{-/-}$ HEK293S cells[30], Fig. 3a–b), we generated a panel of CD1d tetramers by exogenously loading secreted CD1d with one of the following CD1d-Ags or controls: phosphatidylethanolamine (PE), phosphatidylinositol (PI), phosphatidylcholine (PC), phosphatidylserine (PS), sphingomyelin (SM C34:1 or C42:2), sulfatide, lyso-(L)PE, LPC, phosphatidylglycerol (PG), ganglioside GD3, α-GalCer, 3-chlorophenyl-2,2,4,6,7-pentamethyldihydrobenzofuran-5-sulfonate (ClPPBF) [7] or vehicle (tyloxapol) (Fig. 3c). Each tetramer was tested for staining the type II NKT TCR reporter lines (VD3G8, T14, T26A, T26B) and the control NKT lines that expressed the type I NKT15 TCR and the ClPPBF-reactive type II VD1G9 TCR [7] (Fig. 3c). NKT15 and VD1G9 stained only with tetramers carrying their known cognate Ags and not with CD1d-endo. In contrast, amongst all type II NKT lines that were stained with CD1d-endo tetramers (Fig. 2d), T26A and T26B bound CD1d tetramers at similar intensities, regardless of the ligand exogenously added (Fig. 3c**)**, including the bulky GD3 glycolipid [43], whereas T14 and VD3G8 stained less with CD1d-α-GalCer tetramers (Fig. 3c), and in line with Fig. 2d. Thus, in contrast to other NKT lines tested, lipid replacement within CD1d did not markedly affect CD1d-TRAV26 TCR interactions in these systems.

CD1d binding affinity of type II NKT TCRs.

Using surface plasmon resonance (SPR), the affinity of the interaction between three soluble type II NKT TCRs towards CD1d-endo and CD1d bearing sulfatide, GD3 or α-GalCer was examined. The T26A TCR bound to CD1d-endo with an affinity of ~ 7.8 μM and this was not impacted by the type of lipid associated with CD1d, with K_D values ranging from 7.8 μM to 10.6 μM (Fig. 4). Similarly, the T26B TCR bound to CD1d-endo or CD1d with each of the three defined lipids with a similar range of affinities (5.8–15.6 μM) (Fig. 4). Conversely, the T14 TCR exhibited a finer specificity to the lipids presented by CD1d (Fig. 4). Here, whilst the T14 TCR bound to CD1d-endo, CD1d-sulfatide and CD1d-GD3 with K_D values of 13.5, 20.4 and 41.1 μM, respectively, it did not bind to CD1d-□-GalCer (K_D >200 μM), in agreement with the lack of CD1d-□-GalCer tetramer staining of this line (Fig. 2d**)**. Furthermore, none of the tested ligands, including sulfatide, GD3, SM or □-GalCer, enhanced activation of the type II NKT TCR-transduced cell lines measured by CD69 upregulation, whereas □-GalCer elicited stronger activation of the NKT15 type I NKT TCR line, over that elicited by C1R.CD1d or C1R.WT cells (**Fig. S3a**). These responses reflected specific NKT TCR-CD1d interactions, as they were blocked by anti-CD1d, whereas the control AF7 MAIT TCR [44, 45] expressing cells only activated in the presence of 5-OP-RU (**Fig. S3b**). Collectively, these results suggest that the TRAV26$^+$ TCRs interact with CD1d with similar affinity irrespective of the lipid bound.

Structure of the TRAV26$^+$ type II NKT TCR-CD1d-lipid complex.

We determined the crystal structure of the T26A NKT TCR-CD1d-endo ternary complex (Fig. 5a **and Table S1**). The T26A NKT TCR docked ~ 100° across the main axis of the CD1d Ag-binding cleft, being positioned over the 'left' side of the platform on the A'-roof of CD1d, sitting closer to the □$_2$-helix (Fig. 5a). This docking position clearly contrasted to type I NKT TCR-CD1d-lipid binding (Fig. 5d). This 'left-shifted' binding footprint was more reminiscent of the recognition strategy adopted by CD1a autoreactive TCRs [3, 41], CD1d-sulfatide-reactive type II NKT TCRs [19, 20] (Fig. 5c) and some ‘atypical’ human NKT TCRs [22, 23, 24, 25, 26] whereby the TCRs contacted CD1d and the lipid presented.

Mass spectrometry analysis of the T26A TCR-CD1d-endo demonstrated that although mixed lipids were bound, long chain SM (> C40) appeared to be the major species present (Fig. 3a**).** In line with this, we modelled and refined SM (C40:2) as the bound endogenous lipid into the unbiased electron density that was clearly visible within the CD1 cleft (Fig. 6a **& Fig. S2a**). The T26A TCR did not directly contact the protruding headgroup of the lipid bound within the CD1d cleft whereby the most proximal residue to SM was located > 7Å away (Fig. 6b**)**. This distal mode of binding can explain why these TCRs seemingly bind to CD1d in a lipid-independent manner and indeed tolerate binding to CD1d carrying lipids with head groups that differ in size and shape (Figs. 3 and 4). Thus, the TRAV26A$^+$ NKT TCR contacts CD1d itself, which breaks the CD1d-lipid co-recognition paradigm.

Structural basis of TCRa chain bias towards CD1d.

Upon complexation, the buried surface area (BSA) of the T26A NKT TCR-CD1d-endo complex (~ 600 Å^2), fell outside the range for type I NKT TCR-CD1d ternary complexes (760–860 Å^2) and was significantly lower than the mouse type II NKT TCR-CD1d-lipid complexes (~ 1000 Å^2) [19, 20, 21]. The TCRα and TCRβ chains of T26A contributed ~ 75% and ~ 25% of the total BSA at the TCR-CD1d interface, respectively, with both the CDR1α (21% BSA) and CDR2α (16% BSA) loops contributing to the TCR-CD1d interface thereby providing immediate insight into the TRAV26 bias. Conversely, the CDR1β and CDR2β did not interact with the CD1d-endo complex, explaining the broader observation of TRBV gene diversity amongst TRAV26 TCRs (Table 1).

The CDR1α loop sat peripherally above the α2-helix of CD1d whereby Thr30α interacted with Trp160, Gly164, Thr165 and Gln168 residues of CD1d, while Tyr32α stacked against Glu156 and Trp160 (Fig. 6c **and Table S2**). Ser28α contacted only Gln168 while Gly29α contacted Gly164 and Gln168 of CD1d via van der Waals (VDW) and hydrogen bond interactions, respectively (Fig. 6c **and Table S2**). Within the CDR2α loop, Leu51α, Thr52α and Ser53α contacted Asn163 of CD1d and its N-linked glycans (N-acetylglucosamine, NAG) (Fig. 6c **and Table S2**). Further, the germline encoded framework His49α that precedes the CDR2α loop established a VDW interaction with Glu156 in CD1d (**Table S2**). Interestingly, Thr30α, Thr52α and Ser53α mediated several contact points with CD1d and were not conserved in *TRAV26-1* genes, providing molecular insight for why *TRAV26-2* may be over-represented between the two genes amongst CD1d-endo-reactive cells (Table 1).

The CDR3α and CDR3β loops dominated the interactions at the interface with 35% and 25% BSA, respectively (Fig. 6d). The CDR3α and CDR3β loops were positioned more centrally over the CD1d binding-cleft. Here, Arg99β from the CDR3β loop plunged into the CD1d-binding cleft to form VDW interactions with Trp153, Thr157 and Trp160, while Pro100β contacted Glu156 of CD1d (Fig. 6b). The non-germline encoded Gly-Trp motif, which is conserved in 6 out of the 39 TRAV26-2 clones from 4 distinct donors (Fig. 2b **and** Table 2), established multiple contacts with CD1d (Fig. 6d). Whereas in 18 of the 39 TRAV26-2 clones, a Phe residue was present at this position, which constitutes a Gly-Phe motif (Fig. 2b **and** Table 2). Interestingly, this Phe residue was germline-encoded in 7 of the TRAV26-2-TRAJ48^{+} clones across 6 donors. The other 11 clones harbouring the Gly-Phe motif were all non-germline encoded (Fig. 2b **and** Table 2). Conservation of bulky aromatic residues within the CDR3α across 74% of the TRAV26-2^{+} clones may be a key structural determinant governing the TCR docking topology. Further, bias towards Phe may also explain the relatively high occurrence of *TRAV26-2–TRAJ48* rearrangements. The G93X residue was also highly prevalent in both motifs, which might be preferentially selected over other larger amino acids to avoid steric clashes with Trp160 and/or CDR3β residues (Fig. 6d). This finding aligned with the additional patterns observed for TRAV26-2 isolated sequences in positions 6 and 7 (Fig. 2b **bottom**) and emphasized the need for a bulky residue in position 7. Collectively, these results suggested that the germline residues encoded by the *TRAV26-2* gene, and the rearrangement of non-germline-encoded structural motifs to Gly-Phe/Trp, played a key role in determining the docking modality adopted by the T26A TCR over the α2-helix A'-roof of CD1d.

A common mode of recognition of self-lipids by the T26A NKT TCR.

Structural studies on the T26A TCR-CD1d-lipid recognition were extended by loading GD3 into CD1d (**Fig. S2b)** and determining the crystal structure of the ternary complex (Fig. 5). The electron density for the bound GD3 was partially visible whereby only the first glucose moiety of the headgroup and both lipid tails could be modelled (Fig. 6e **and Fig. S2c**). The crystal structure revealed a nearly identical docking mode to that of CD1d-endo complex that was modelled as CD1d-SM (Fig. 5). The majority of the molecular interactions at the T26A NKT TCR-CD1d-GD3 interface were also conserved (**Fig. S2d-e and Table S3**). Indeed, the T26A NKT TCR did not contact the GD3 lipid, as the most proximal TCR residue, Arg99β from the CDR3β, was 10Å away from the glucose moiety (Fig. 6f). Other sphingolipid Ags such as α-GalCer would be expected to produce similar observations (**Fig. S2f**). Collectively, our structural analysis of the T26A type II NKT TCR suggests a new molecular paradigm for CD1d recognition whereby the type II TRAV26^{+} NKT TCR can bind CD1d in a lipid-independent manner.

Molecular footprint of TRAV26 type II NKT TCRs onto CD1d.

Having established that lipid Ags had little impact on TRAV26^{+} TCRs binding to CD1d, the next step was to assess their functional CD1d docking footprints. Here, C1R cell lines overexpressing wild type CD1d or alanine-substituted CD1d mutants targeting solvent-exposed residues of CD1d [7] were used to test their ability to stimulate the TRAV26^{+} and TRAV26^{-} TCR-transduced cell lines (Fig. 7). CD69 upregulation on the NKT15 TCR control line was inhibited by the alanine mutations of Glu83, Val147, Lys86, and Met87, all positioned near to the F'-portal of CD1d, consistent with our previous results [7] and the 'right-shifted' parallel docking strategy adopted by type I NKT TCR(s) [35] (Fig. 7). In contrast, the three TRAV26^{+} TCR transduced cell lines were not impacted by those mutations but were inhibited (> 75%) by mutations of two CD1d residues Gln62 and Trp160, located distant from the F'-portal, where Ags protrude. These data complement the structural data showing that TRAV26^{+} TCRs bind the A'-roof. The impact of the CD1d alanine mutant scan was similar, but not identical, across the three TRAV26 TCR lines. This outcome likely reflects differences in CDR3α and TCRβ chain pairing, and their influence on CD1d-binding.

Activation of both TRAV26^{-} TCR transduced lines (T14 and VD3G8) was severely impacted by mutations of Trp160 and His68, which sit in the A'-roof of CD1d, in addition to other residues closer to the Ag portal, spanning to the F'-roof. Specifically, T14 was moderately inhibited by mutations of Val72, Thr157, Glu83 and Val147 and VD3G8 impacted by Thr157, Glu83, whereas Arg79Ala mutation led to enhanced activation, suggesting that Arg79 interferes with optimal VD3G8 TCR binding to CD1d. Thus, these TRAV26^{-} TCRs appeared to dock more centrally and over the Ag portal, which likely reflects their differences in sensing CD1d-bound ligands (Figs. 2c, 3c and 4), unlike the extreme A'-roof CD1d-docking by TRAV26^{+} TCRs. Collectively, these data suggest that TRAV26^{+} NKT TCRs bind to CD1d in a left-shifted approach and ligand-independent manner.

DISCUSSION

Currently, the CD1d-restricted repertoire is thought to comprise a highly conserved population of type I NKT cells, and a group of diverse type II NKT cells. Here, we identify a public population of type II NKT cells defined by a TRAV26 TCR bias and a conserved CDR3a motif and we provide detailed molecular insight into their mode of lipid-independent CD1d recognition. With wider implementation of CD1 tetramers to systematically investigate TCR repertoires, we are increasingly detecting conserved patterns and public TCR usage for particular CD1-Ag pairs [7, 46, 47, 48, 49]. A general view emerging from these studies is that NKT cells are not exclusively represented by a public TCR, but instead that non-polymorphic CD1 proteins generate an underlying network of T cells shared across donors, with many conserved families of TCRs and Ags.

The epitope for the TRAV26 TCR is CD1d itself rather than a defined lipid. Thus, an exposed A'-roof is likely a common or nearly universal epitope in humans, which could account for the several distinct TRAV26-TRAJ48^{+} T cell clones seen in every donor tested here. These data connect to a prior study where two distinct *TRAV26-2* encoded TCRs (*TRAV26-2—TRAJ48* and *TRAV26-2—TRAJ44*) were reported among 14 *TRAV10^{-}TRAJ18^{-}TRBV25^{-}* TCRs isolated with CD1d-a-GalCer tetramers [25], albeit not recognised as a conserved motif through the strategy employed at the time. The Ag-independent mode of CD1d recognition by germline-encoded TRAV26 TCR residues and a conserved CDR3α motif raises interesting questions about the evolutionary pressures that lead to the conservation of TCRs to act as pattern recognition receptors against CD1d.

Thus, our results also suggest that some type II NKT cells might be poised to sense overall changes in surface expression of the Ag-presenting molecule CD1d, rather than the lipid-Ag itself. Accordingly, changes in surface expression levels of CD1d have been shown to impact NKT cell function [50] and are often associated with infection [51, 52, 53, 54], cancer [55] and autoimmunity [56]. For example, hepatocytes that are chronically infected with Hepatitis C display high CD1d surface expression relative to healthy tissue or other liver disease, to levels that resemble those of C1R.CD1d transfectants published within the same study to elicit IFN-γ release from intrahepatic CD1d-reactive T cells (Type II NKT) [57]. Similarly, another study demonstrated that CD1d overexpression can be targeted by mouse CD1d-reactive Vγ4^{+} T cells, promoting viral myocarditis *sequela* of coxsackievirus infections [58]. Whether these physiological contexts can lead to activation of TRAV26^{+} NKT cells is an important question for further exploration.

Whilst some type II NKT clones can display lipid-Ag specificity [19, 20, 21, 59, 60] and mount lipid Ag-driven responses [12, 13, 61], other type II NKT cells also retain the ability to recognise CD1d carrying multiple self-Ags [4, 27, 28, 59] possibly as a strategy to sense early stress signals in an innate-like fashion [55, 62, 63, 64]. Self-reactive profiles have been reported amongst other CD1-restricted lipid-reactive T cells in humans [2] and ligand-independent interactions have been described for CD1a [37, 65], CD1b [66], CD1c [38] and CD1d [67], and MR1 [68], where the structural mechanism in part relies on smaller Ags hiding inside antigen-binding clefts (particularly for the CD1 system) [3]. However, non-permissive lipids, such as long chain SM (42:2), bound by CD1a or CD1c can prevent docking of endo-reactive TCRs[38, 41, 69]. Here, we show that TRAV26 TCRs engage CD1d when displaying a variety of headgroup-containing lipids, over the extreme side of the A´-roof, without contacting the protruding headgroups. Accordingly, both the α1 and α2helixes of the A´-roof are heavily contacted by TRAV26-2 TCR α-chain and may form an anchor region within CD1d targeted by non-type I NKT TCRs, including the 'atypical' CD1d-α-GalCer reactive NKT TCRs (*TRAV10–TRAJ18^{-}*) [22, 23, 24, 25, 26], CD1d-benzofuran-self-lipid reactive type II NKT TCRs [7], and the murine sulfatide reactive TCRs[19, 20]. However, all previously structurally described CD1d interactions involve NKT TCR co-engagement of CD1d and their cognate lipid, which contrasts our novel study of TRAV26^{+} TCRs.

Limitations of the Study and future directions

The TCR patterns identified among CD1d-endo reactive clones followed in vitro expansion of sorted cells, which is commonly used in studies of rare populations [7, 22, 24, 32] and was necessary for us to confidently identify these cells. While it is possible this may have altered the representation of some TCRs within the population, the expansion is based on anti-CD3 stimulation and therefore should not inherently favour any particular TCRs. While this approach precludes addressing immune-function ex vivo, nonetheless, we have shown that expanded TRAV26 cells are capable of producing a range of cytokines, in particular TNF and IFNγ, implying that these cells have pro-inflammatory potential and future studies will investigate their contributions to various health and disease states. It will also be important to address the intrinsic or extrinsic regulatory mechanisms that define the activity and immune function of TRAV26, including their reliance on secondary signals such as cytokines [64] or other receptors such as NK receptors [70], which can play a role in modulating activation status in a TCR-independent manner. Most importantly, our findings suggest that TRAV26 cells are highly represented within the CD1d-endo reactive population and are present as a public TCR in essentially all individuals tested. The potential significance of these observations is highlighted by an earlier study where we revealed the TRAV12-TRAJ6 type II NKT TCR motif [7], specifically reactive to small benzofuran-like molecules bound by CD1d. That TCR motif was subsequently implicated in Crohn's disease [71, 72] where the cells were named Crohn's-associated invariant T cells (CAIT cells), which is now underpinning studies to investigate the contributions of CAIT cells and the CD1d axis to this disease.

Several candidate therapies have explored the immunomodulating potential of type I NKT cells, with ongoing trials also including CAR-type I NKT cell allogenic and adoptive therapies [73]. The findings of this study may offer new avenues to modulate immune responses through the monomorphic protein CD1d and overcome existing limitations of current trials, that require a-GalCer co-delivery to allow type I NKT-activation [74]. Moreover, our observation that TRAV26 TCRs retain their ability to recognise the complex glycan headgroup of GD3 loaded onto CD1d, which inhibits type I NKT responses [43], flags their potential exploration in therapies against GD3-expressing cancers. These findings further highlight the possibility of future immunomodulation agonists, antagonists or anti-TCR antibodies to selectively manipulate these public TRAV26^{+} type II NKT cells.

METHODS

Flow cytometry. Buffy coats from healthy blood donors were obtained from the Australian Red Cross Blood Service (agreement 13-04VIC-07), and all experiments were conducted in accordance with the University of Melbourne Human Research and Ethics committee guidelines (approval number 1035100). PBMCs were prepared through density gradient centrifugation using Ficoll-Paque (GE Healthcare). Cells were incubated for 10 min with Fc-receptor block (BD Pharmingen) and 5% (v/v) mouse serum, followed by CD1d-endo tetramers for 30min on ice. Where described, CD1d–endo tetramer^{+} cells were enriched by TAME, using anti-phycoerythrin (PE) magnetic beads and LS columns (Miltenyi Biotec), and stained with secondary antibodies including: CD3ε (UCHT1, eBioscience and Becton Dickinson), CD4 (RPA-T4, BD Pharmingen), CD8α (SK1, BD Pharmingen), CD19 (HIB19, BioLegend), CD14 (MφP9, BD Pharmingen), TCRγδ (11F2, BD Pharmingen), and 7-aminoactinomycin D (7AAD) viability dye (Sigma). CD3^{+} CD1d–endo tetramer^{+} cells were sorted using a FACSAria (BD Biosciences). When reassessed immediately after the first-sort, purities ranged 13–65%. Where described, sorted cells were then expanded for 18–21 days, whereby in the first two they were exposed to plate bound anti-CD3 (10 μg/mL, UCHT1, BD Pharmingen) and anti-CD28 (5μg/mL, CD28.2, BD Pharmingen), in

the presence of IL-2 (20 U/mL, Prepotech) IL-7 (50 ng/mL, eBioscience) and IL-15 (40 pg/mL), in complete RPMI-1640 supplemented with 10% (v/v) FBS (JRH Biosciences), penicillin (100 U/ml, Sigma), streptomycin (100 µg/ml), Glutamax (2 mM), sodium pyruvate (1 mM), nonessential amino acids (0.1 mM), HEPES buffer (15 mM, pH 7.2–7.5) (all from Invitrogen, Life Technologies) and 2-mercaptoethanol (50 µM, Sigma). After expansion cells were re-stained with CD1d-endo tetramers alone, followed by surface antibodies and secondary CD1d-endo as well as CD1d-α-GalCer tetramer staining. These sorted and expanded $CD3^+$CD1d-endo $tetramer^+$ cells were then index-sorted as single cells for TCR sequencing. Data analysis was completed using FlowJo (Tree Star Inc), and graphs generated using GraphPad Prism.

Lipids. α-GalCer C24:1 (PBS44) used for CD1d tetramers was kindly provided by P. Savage (Brigham Young University). α-GalCer C26:0 used for cellular activation assays was supplied by Alexis Biochemicals, and SM C42:2, SM C34:1, PC C42:1; sulfatide C42:2, PE C36:1, PS C36:1 PC C36:1, PC C42:2, PI C36:1, PG C36:1, LPE C18:1, LPC C18:1, pLPE C18:1 from Avanti Polar Lipids. Disialo-ganglioside GD3 C34:1 was purchased from Matreya. CD1d-ligands were dissolved in tris buffer saline (TBS) alone (pH 8) or TBS containing 0.05% v/v tyloxapol (Sigma), or buffer containing 0.5% v/v tween-20, 57 mg/ml sucrose and 7.5 mg/ml histidine, and exogenously loaded overnight into soluble biotinylated CD1d at 12-fold molar excess (except for α-GalCer - loaded at 6-fold), prior to tetramerization.

Identification of the NKT TCRs. $CD3^+$CD1d-endo $tetramer^+$ cells were single-cell sorted from CD1d-endo tetramer-enriched and culture-expanded NKT cells (as described above), and cDNA generated using 0.1% Triton X-100 (Invitrogen) and SuperScript VILO according to manufacturer's instructions. Paired TCRα and TCRβ or TCRγ and TCRδ chain-transcripts were amplified as previously described [31]. PCR products were sequenced at the AGRF facility (Australia) and analysed using IMGT [75]. TCR nomenclature is presented in accordance with the IMGT guidelines. Unproductive TCR gene rearrangements were excluded from analysis. The first 10 amino acids of the CDR3α of TRAV26 TCRs shown in Fig. 2b were aligned using Logomaker [76].

Generation of stable cell lines and stimulation assay. TCR constructs containing the full-length TCRα and TCRβ or TCRδ and TCRγ chains separated by a 2A-cleavable linker were synthesized (Genscript) and cloned into the pMIGII plasmid. TCR-deficient SKW3.β2m$^{-/-}$ cells were retrovirally transduced with the TCR and a 2A-cleavable human CD3 [77], plus the packaging vectors pEQ-Pam-3-E pVSV-G and using HEK293T cells as packaging cells and FUGENE 6 (Promega), as previously described [78]. The pMIGII, expression and packaging vectors were provided by Dr. Dario Vignali (St. Jude's Research Hospital, USA), and the CD3 expression vector was provided by Prof. Stephen Turner (Monash University, Australia). CD3(GFP)^{hi} cells were sorted and assessed for their ability to bind CD1d tetramers by flow cytometry. For Fig. 2C, HEK293T cells were transiently transduced with CD3 and TCR vectors in the same manner but in the absence of packaging vectors and assessed after 48h for CD3/TCR expression and CD1d-tetramer binding by flow cytometry. C1R cells were transduced to express human CD1d or mutated versions of CD1d, akin to SKW3.β2m$^{-/-}$ cells, and purified using flow cytometric sorting to produce stable cells lines expressing similar surface levels of CD1d [7].

Activation assays. For stimulation assays, TCR-expressing SKW3.β2m$^{-/-}$ cells were co-cultured overnight in complete RPMI (as described above), with or without C1R cells (either C1R.WT, C1R.CD1d or C1R.β2m$^{-/-}$) cells, with α-GalCer C26:0 at 1 µg/mL, sulfatide C42:2, SM C42:2 or GD3 C34:1 at 20 µg/mL, or vehicle controls, and with either anti-CD1d (51.1, Biolegend), isotype control antibody (MPC-11 or MG2b-57, Biolegend) or media alone, in round-bottom 96-well plates. Activation of TCR-transduced cells was analysed by flow cytometry for CD69 upregulation using anti-CD69 (FN50, BD Pharmingen). For functional analysis of PBMCs, CD1d-endo tetramer positive or negative cells that had been FACS-sort expanded for 20 days as described above were exposed to 10 ng/mL PMA, 1 µg/mL Ionomicyn and 1/1000, Golgi stop (1/500, BD Pharmingen), Brefeldin A (1/1000, BD Pharmingen) and for 4h in complete media prior to assessment of intracellular cytokine production using BD Cytofix/Cytoperm kit (BD Biosciences), anti-TNF (MAb11, BD Pharmingen), anti-IFNg (4S.B3, Biolegend) and anti-IL-13 (JES10-5A2, BD Pharmingen).

CD1d and NKT TCRs production and purification. The human CD1d sequence encoding for truncated recombinant human CD1d ectodomain harbouring a C-terminal BirA and six-histidine (GSGLNDIFEAQKIEWHEHHHHHH) affinity tags, and β2-microglobulin, both in separate pHLsec vectors, were co-transfected into GnTI$^{-/-}$ HEK293S for expression using polyethyleneimine as described[7, 79]. The soluble CD1d glycoprotein was purified by Ni/NTA affinity purification followed by size-exclusion chromatography using a Superdex 200 16/60 column (GE Healthcare). CD1d was enzymatically biotinylated using biotin ligase (produced in-house) and further purified by size-exclusion chromatography using a Superdex-75 16/60 gel-filtration column (GE healthcare), followed by storage at − 80°C. Biotinylated CD1d proteins carrying endogenous lipids (endo), or exogenously loaded *in vitro* (as described in the lipids section) were tetramerised using SAV-PE or SVA-BV421 (Biolegend).

The genes encoding the T26A (TRAV26-TRBV19), T14 (TRAV14-TRBV19) and T26B (TRAV26-TRBV13) TCRs after codon optimization, were synthesized (Genscript) and cloned into the expression vector pET30 (Novagen). The TCRα and TCRβ chains of the three NKT TCRs were expressed in *Escherichia coli* strain BL21 and purified as inclusion bodies (IBs) as described[17]. The IBs were resuspended in the following buffer: 8 M urea, 0 mM Tris-HCl-pH 8.0, 0.5 mM Na-EDTA, 1 mM DTT. The three TCRs were refolded by dilution in a solution containing 5 M urea, 0.1 M Tris-HCl-pH 8.0, 2 mM Na-EDTA, 400 mM L-arginine-HCl, 0.5 mM oxidized glutathione, 5 mM reduced glutathione. The refolding solutions were then dialyzed against 10mM Tris pH 8.0. The NKT TCRs were purified by Diethyl aminoethyl (DEAE) anion exchange, size exclusion and HiTrap-Q anion-exchange chromatography techniques.

In vitro loading of lipids into human CD1d for crystallography and SPR. Lipid solutions of GD3, sulfatide and α-GalCer were prepared at 1 mg/mL in 0.5% tyloxapol. Prior to lipid loading, the lipid solutions were sonicated for 30 mins and immediately transferred to a 60°C water bath for 1 min and left to cool at room temperature for 1 min. The lipids GD3,sulfatide were then added directly to CD1d-endo at a 3–6:1 molar ratio and incubated in 10ml TBS150 (Tris buffered saline, 150mM NaCl, 10mM Tris pH 8.0) at room temperature for 15 h. The lipid-loaded CD1d were then purified by MonoQ anion-exchange chromatography (GE Healthcare). α-GalCer was loaded at a 6:1 molar ratio into the purified CD1d-GD3 binary complex and purified by MonoQ anion-exchange chromatography.

Purification of TCR-CD1d-endo complex and mass spectrometry analysis. The T26A, T26B or T14 TCRs were incubated with CD1d-endo for 16 hours. The mixture was then subjected to gel filtration on a Superdex 200 16/60 column (GE Healthcare) to isolate the TCR-CD1d-endo ternary complex. The 'TCR trap' assay was performed as previously described with minor changes [41, 42]. The gel filtration protein fractions were subjected to Bligh and Dyer extraction, and the extracted lipids were initially analysed by shotgun nano-electrospray on a Thermo Fisher LXQ Ion Trap mass spectrometer. For the semi-quantitative, high resolution mass analysis, the lipid eluents were normalized to 20 µM based on the input proteins and 10 µl was injected into a reversed-phase HPLC system (Agilent Poroshell EC-C18 column, 1.9-micron, 3 x 50 mm) with an Agilent 6520 Accurate-Mass Q-TOF mass spectrometer. The gradient conditions were modified from a prior method (Klooster, elife, 2020): the mobile phases were (A) 2 mM ammonium formate in 90/10 methanol/water (v:v) and (B) 2 mM ammonium formate in 90/10/0.1 1-propanol/cyclohexane/water (v:v:v). The 30-minute gradients were: 0–4 min of 100% A, 4–13 min from 100% A to 100% B, 13–18 min of 100% B, 18–20 min from 100% B to 100% A, and 20–30 min of 100% A.

Surface plasmon resonance (SPR) measurements and analysis. All the experiments were performed at 25°C on Biacore 3000 and T200 using HBS buffer (10 mM HEPES- HCl - pH 7.4, 150 mM NaCl). Biotinylated CD1d-endo, CD1d-sulfatide, CD1d-α-GalCer and CD1d-GD3 were coupled (~ 3,000 RU) onto a research-grade SA chip and the four TCRs were applied at a flow rate of 5 µl/min. The first flow cell was left blank and was used as a reference for subsequent analysis. The final response was calculated by subtraction of the response of the streptavidin-coated chip alone from that of TCR-CD1d-lipid interaction. BIAevaluation Version 3.1 (Biacore AB) and Biacore T200 Evaluation Software 3.2.1 were used to fit the data to the 1:1 Langmuir binding model. GraphPad Prism 10 was used for data presentation.

Crystallization, structure determination and refinement. The T26A NKT TCR-CD1d-endo (7 mg/ml) and the T26A NKT TCR-CD1d-GD3 (7 mg/ml) ternary complexes were both crystallized in 16–24% PEG 3350, 0.1M sodium citrate, 0.1 M citrate-bis-Tris-pH 7 using the hanging-drop diffusion method at 20°C. The crystals were cryoprotected in 10% glycerol and flash-frozen in liquid nitrogen. Crystallographic data were collected at the MX2 beamline (Australian Synchrotron). Data were processed with the XDS software [80] and scaled using SCALA from the CCP4 suite of programs [81]. The crystal structure of the T26A NKT TCR-CD1d-endo ternary complex was determined by molecular replacement method using PHASER [82] and the TCRα (Protein Data Bank accession code: 6RSY) [83], TCRβ (PDB accession code: 5JHD) [84] and human CD1d–α-GalCer (PDB accession code: 2PO6) [35] as search models. The crystal structure of the T26A NKT TCR-CD1d-GD3 ternary complex was also solved by molecular replacement using PHASER and the T26A NKT TCR-CD1d-endo ternary complex as a search model. Both ternary complexes were refined using the Phenix refinement program [85], and the COOT program [86] was used for macromolecular model building. The quality of the structures was validated using the Research Collaboratory for Structural Bioinformatics Protein Data Bank Data Validation and Deposition Services. All structural diagrams were created using PyMOL [87].

Declarations

Data Availability

The coordinates of the T26A NKT TCR-CD1d-SM and T26A NKT TCR-CD1d-GD3 ternary complexes were deposited in the Protein Data Bank (PDB) database under the accession codes 8SGB and 8SGM, respectively. All remaining data are available within the article and associated files and upon reasonable request from the corresponding authors. Source data are provided in this paper.

Acknowledgments

We are grateful to Paul Savage (Brigham Young University, UT, USA) and Spencer Williams (Bio21, University of Melbourne, Australia) for providing lipid antigens, and Dr Sidonia Eckle for providing the MAIT TCR control SKW3 line (clone AF7). We thank staff from the Flow Cytometry facility at the Peter Doherty Institute, David Price (statistician at the Doherty Institute) for advice on data distribution display *and staff at the MX2 beamline at the Australian Synchrotron and* Macromolecular Crystallization Platform [88]. This work was supported by a University of Melbourne Early Career Researcher grant (C. F. A.), the National Health and Medical Research Council of Australia (NHMRC: 1145373, 1113293, 200891, 31106741, 2008913 and 2029256), the Australian Research Council (ARC: DP170104386, DP210103064 and DP220102402). D. G. P. was supported by a CSL Centenary Fellowship and is now supported by a Sylvia & Charles Viertel Fellowship; D. I. G. was supported by an NHMRC Senior Principal Research Fellowship (1117766) and subsequently, an NHMRC Investigator Award (2008913). J. R. is supported by an NMHRC Investigator Award (2008981). D. B. M. is supported by the NIH (AR 048632, AI 049313). D.B.M and J.R. are supported by a Welcome Trust Discovery Award.

Author contributions

K. C. Y. P. and C. M. H. are joint co-first authors who along with, T. Y. C., R. L., E. B., C. V. N-R., C. S., S. J. J. R, C. M., A.P.U. and C. F. A. contributed to data generation, data analysis and/or paper editing. D. B. M., J. R., D. I. G, D. G. P., J. L. N. and C. F. A. contributed to project conceptualisation, funding acquisition, data interpretation, paper reviewing and editing. K. C. Y. P. and C. M. H., J. L. N. and C. F. A. co-wrote the initial draft.

Conflicts of interest

D. I. G and C. F. A hold two patents on CD1-targetting for immune modulation.

References

1. Godfrey DI, MacDonald HR, Kronenberg M, Smyth MJ (2004) Van Kaer, L. NKT cells: what's in a name? Nat Rev Immunol 4:231–237
2. Godfrey DI, Uldrich AP, McCluskey J, Rossjohn J, Moody DB (2015) The burgeoning family of unconventional T cells. Nat Immunol 16:1114–1123

3. Cao TP et al (2024) A structural perspective of how T cell receptors recognize the CD1 family of lipid antigen-presenting molecules. J Biol Chem 300:107511
4. Cardell S et al (1995) CD1-restricted CD4 + T cells in major histocompatibility complex class II-deficient mice. J Exp Med 182:993–1004
5. Chiu YH et al (1999) Distinct subsets of CD1d-restricted T cells recognize self-antigens loaded in different cellular compartments. J Exp Med 189:103–110
6. Behar SM, Podrebarac TA, Roy CJ, Wang CR, Brenner MB (1999) Diverse TCRs recognize murine CD1. J Immunol 162:161–167
7. Almeida CF et al (2021) Benzofuran sulfonates and small self-lipid antigens activate type II NKT cells via CD1d. Proc Natl Acad Sci U S A 118:e2104420118
8. Singh AK, Tripathi P, Cardell SL (2018) Type II NKT Cells: An Elusive Population With Immunoregulatory Properties. Front Immunol 9:1969
9. Dhodapkar MV, Kumar V (2017) Type II NKT Cells and Their Emerging Role in Health and Disease. J Immunol 198:1015–1021
10. Nair S et al (2015) Type II NKT-TFH cells against Gaucher lipids regulate B-cell immunity and inflammation. Blood 125:1256–1271
11. Zhou D et al (2004) Lysosomal glycosphingolipid recognition by NKT cells. Science 306:1786–1789
12. Zeissig S et al (2012) Hepatitis B virus-induced lipid alterations contribute to natural killer T cell-dependent protective immunity. Nat Med 18:1060–1068
13. Chang DH et al (2008) Inflammation-associated lysophospholipids as ligands for CD1d-restricted T cells in human cancer. Blood 112:1308–1316
14. Exley MA et al (2001) A major fraction of human bone marrow lymphocytes are Th2-like CD1d-reactive T cells that can suppress mixed lymphocyte responses. J Immunol 167:5531–5534
15. Fuss IJ et al (2004) Nonclassical CD1d-restricted NK T cells that produce IL-13 characterize an atypical Th2 response in ulcerative colitis. J Clin Investig 113:1490–1497
16. Exley MA et al (2002) Cutting edge: Compartmentalization of Th1-like noninvariant CD1d-reactive T cells in hepatitis C virus-infected liver. J Immunol 168:1519–1523
17. Kjer-Nielsen L et al (2006) A structural basis for selection and cross-species reactivity of the semi-invariant NKT cell receptor in CD1d/glycolipid recognition. J Exp Med 203:661–673
18. Pellicci DG et al (2009) Differential recognition of CD1d-alpha-galactosyl ceramide by the V beta 8.2 and V beta 7 semi-invariant NKT T cell receptors. Immunity 31:47–59
19. Girardi E et al (2012) Type II natural killer T cells use features of both innate-like and conventional T cells to recognize sulfatide self antigens. Nat Immunol 13:851–856
20. Patel O et al (2012) Recognition of CD1d-sulfatide mediated by a type II natural killer T cell antigen receptor. Nat Immunol 13:857–863
21. Almeida CF et al (2019) Distinct CD1d docking strategies exhibited by diverse Type II NKT cell receptors. Nat Commun 10:5242
22. Uldrich AP et al (2013) CD1d-lipid antigen recognition by the gammadelta TCR. Nat Immunol 14:1137–1145
23. Luoma AM et al (2013) Crystal structure of Vdelta1 T cell receptor in complex with CD1d-sulfatide shows MHC-like recognition of a self-lipid by human gammadelta T cells. Immunity 39:1032–1042
24. Pellicci DG et al (2014) The molecular bases of delta/alphabeta T cell-mediated antigen recognition. J Exp Med 211:2599–2615
25. Le Nours J et al (2016) Atypical natural killer T-cell receptor recognition of CD1d-lipid antigens. Nat Commun 7:10570
26. Lopez-Sagaseta J, Kung JE, Savage PB, Gumperz J, Adams EJ (2012) The molecular basis for recognition of CD1d/alpha-galactosylceramide by a human non-Valpha24 T cell receptor. PLoS Biol 10:e1001412
27. Burdin N et al (1998) Selective ability of mouse CD1 to present glycolipids: alpha-galactosylceramide specifically stimulates V alpha 14 + NK T lymphocytes. J Immunol 161:3271–3281
28. Park SH et al (2001) The mouse CD1d-restricted repertoire is dominated by a few autoreactive T cell receptor families. J Exp Med 193:893–904
29. Haig NA et al (2011) Identification of self-lipids presented by CD1c and CD1d proteins. J Biol Chem 286:37692–37701
30. Huang S et al (2023) CD1 lipidomes reveal lipid-binding motifs and size-based antigen-display mechanisms. Cell 186:4583–4596e4513
31. Dash P et al (2011) Paired analysis of TCRalpha and TCRbeta chains at the single-cell level in mice. J Clin Investig 121:288–295
32. Gherardin NA et al (2021) CD36 family members are TCR-independent ligands for CD1 antigen-presenting molecules. Sci Immunol 6:eabg4176
33. Bai L et al (2012) The majority of CD1d-sulfatide-specific T cells in human blood use a semiinvariant Vdelta1 TCR. Eur J Immunol 42:2505–2510
34. Roy S et al (2016) Molecular Analysis of Lipid-Reactive Vdelta1 gammadelta T Cells Identified by CD1c Tetramers. J Immunol 196:1933–1942
35. Borg NA et al (2007) CD1d-lipid-antigen recognition by the semi-invariant NKT T-cell receptor. Nature 448:44–49
36. de Jong A et al (2014) CD1a-autoreactive T cells recognize natural skin oils that function as headless antigens. Nat Immunol 15:177–185
37. Cotton RN et al (2021) Human skin is colonized by T cells that recognize CD1a independently of lipid. J Clin Investig 131:e140706
38. Wun KS et al (2018) T cell autoreactivity directed toward CD1c itself rather than toward carried self lipids. Nat Immunol 19:397–406
39. Zajonc DM et al (2005) Structural basis for CD1d presentation of a sulfatide derived from myelin and its implications for autoimmunity. J Exp Med 202:1517–1526
40. Gumperz JE et al (2000) Murine CD1d-restricted T cell recognition of cellular lipids. Immunity 12:211–221
41. Birkinshaw RW et al (2015) alphabeta T cell antigen receptor recognition of CD1a presenting self lipid ligands. Nat Immunol 16:258–266
42. Brennan PJ et al (2017) Structural determination of lipid antigens captured at the CD1d-T-cell receptor interface. Proc Natl Acad Sci U S A 114:8348–8353

43. Webb TJ et al (2012) Molecular identification of GD3 as a suppressor of the innate immune response in ovarian cancer. Cancer Res 72:3744–3752
44. Tilloy F et al (1999) An invariant T cell receptor alpha chain defines a novel TAP-independent major histocompatibility complex class Ib-restricted alpha/beta T cell subpopulation in mammals. J Exp Med 189:1907–1921
45. Eckle SB et al (2014) A molecular basis underpinning the T cell receptor heterogeneity of mucosal-associated invariant T cells. J Exp Med 211:1585–1600
46. Van Rhijn I et al (2013) A conserved human T cell population targets mycobacterial antigens presented by CD1b. Nat Immunol 14:706–713
47. Van Rhijn I et al (2014) TCR bias and affinity define two compartments of the CD1b-glycolipid-specific T Cell repertoire. J Immunol 192:4054–4060
48. Guo T et al (2018) A Subset of Human Autoreactive CD1c-Restricted T Cells Preferentially Expresses TRBV4-1(+) TCRs. J Immunol 200:500–511
49. Roy S et al (2014) Molecular basis of mycobacterial lipid antigen presentation by CD1c and its recognition by alphabeta T cells. Proc Natl Acad Sci U S A 111:E4648–4657
50. Falcone M et al (2004) Up-regulation of CD1d expression restores the immunoregulatory function of NKT cells and prevents autoimmune diabetes in nonobese diabetic mice. J Immunol 172:5908–5916
51. Yuan W, Dasgupta A, Cresswell P (2006) Herpes simplex virus evades natural killer T cell recognition by suppressing CD1d recycling. Nat Immunol 7:835–842
52. Chung BK et al (2013) Innate immune control of EBV-infected B cells by invariant natural killer T cells. Blood 122:2600–2608
53. Sanchez DJ, Gumperz JE, Ganem D (2005) Regulation of CD1d expression and function by a herpesvirus infection. J Clin Investig 115:1369–1378
54. Durante-Mangoni E et al (2004) Hepatic CD1d expression in hepatitis C virus infection and recognition by resident proinflammatory CD1d-reactive T cells. J Immunol 173:2159–2166
55. Skold M, Xiong X, Illarionov PA, Besra GS, Behar SM (2005) Interplay of cytokines and microbial signals in regulation of CD1d expression and NKT cell activation. J Immunol 175:3584–3593
56. Bagchi S, Genardi S, Wang CR (2018) Linking CD1-Restricted T Cells With Autoimmunity and Dyslipidemia: Lipid Levels Matter. Front Immunol 9:1616
57. Yanagisawa K et al (2013) Ex vivo analysis of resident hepatic pro-inflammatory CD1d-reactive T cells and hepatocyte surface CD1d expression in hepatitis C. J Viral Hepat 20:556–565
58. Huber S, Sartini D, Exley M (2003) Role of CD1d in coxsackievirus B3-induced myocarditis. J Immunol 170:3147–3153
59. Tatituri RV et al (2013) Recognition of microbial and mammalian phospholipid antigens by NKT cells with diverse TCRs. Proc Natl Acad Sci U S A 110:1827–1832
60. Wolf BJ et al (2015) Identification of a Potent Microbial Lipid Antigen for Diverse NKT Cells. J Immunol 195:2540–2551
61. Maricic I, Girardi E, Zajonc DM, Kumar V (2014) Recognition of Lysophosphatidylcholine by Type II NKT Cells and Protection from an Inflammatory Liver Disease. J Immunol 193:4580–4589
62. Brennan PJ et al (2011) Invariant natural killer T cells recognize lipid self antigen induced by microbial danger signals. Nat Immunol 12:1202–1211
63. Mattner J et al (2005) Exogenous and endogenous glycolipid antigens activate NKT cells during microbial infections. Nature 434:525–529
64. Brigl M, Bry L, Kent SC, Gumperz JE, Brenner MB (2003) Mechanism of CD1d-restricted natural killer T cell activation during microbial infection. Nat Immunol 4:1230–1237
65. de Jong A et al (2010) CD1a-autoreactive T cells are a normal component of the human alphabeta T cell repertoire. Nat Immunol 11:1102–1109
66. Reijneveld JF et al (2020) Human gammadelta T cells recognize CD1b by two distinct mechanisms. Proc Natl Acad Sci U S A 117:22944–22952
67. Cheng TY et al (2024) Lipidomic scanning of self-lipids identifies headless antigens for natural killer T cells. Proc Natl Acad Sci U S A 121:e2321686121
68. Le Nours J et al (2019) A class of gammadelta T cell receptors recognize the underside of the antigen-presenting molecule MR1. Science 366:1522–1527
69. Cotton RN et al (2021) CD1a selectively captures endogenous cellular lipids that broadly block T cell response. J Exp Med 218:e20202699
70. Kuylenstierna C et al (2011) NKG2D performs two functions in invariant NKT cells: direct TCR-independent activation of NK-like cytolysis and co-stimulation of activation by CD1d. Eur J Immunol 41:1913–1923
71. Minervina AA et al (2023) Crohn's-associated invariant T cells (CAITs) recognise small sulfonate molecules on CD1d. Gut 73:205–206
72. Rosati E et al (2022) A novel unconventional T cell population enriched in Crohn's disease. Gut 71:2194–2204
73. Exley MA, Dellabona P, Casorati G (2021) Exploiting CD1-restricted T cells for clinical benefit. Mol Immunol 132:126–131
74. Godfrey DI, Le Nours J, Andrews DM, Uldrich AP, Rossjohn J (2018) Unconventional T Cell Targets for Cancer Immunotherapy. Immunity 48:453–473
75. Lefranc MP et al (1998) IMGT, the International ImMunoGeneTics database. Nucleic Acids Res 26:297–303
76. Tareen A, Kinney JB (2020) Logomaker: beautiful sequence logos in Python. Bioinformatics 36:2272–2274
77. Szymczak AL et al (2004) Correction of multi-gene deficiency in vivo using a single 'self-cleaving' 2A peptide-based retroviral vector. Nat Biotechnol 22:589–594
78. Holst J et al (2006) Generation of T-cell receptor retrogenic mice. Nat Protoc 1:406–417
79. Aricescu AR et al (2006) Eukaryotic expression: developments for structural proteomics. Acta Crystallogr D Biol Crystallogr 62:1114–1124
80. Kabsch W (2010) Integration, scaling, space-group assignment and post-refinement. Acta Crystallogr D Biol Crystallogr 66:133–144
81. Winn MD et al (2011) Overview of the CCP4 suite and current developments. Acta Crystallogr D 67:235–242
82. McCoy AJ et al (2007) Phaser crystallographic software. J Appl Crystallogr 40:658–674

83. Holland CJ et al (2020) Specificity of bispecific T cell receptors and antibodies targeting peptide-HLA. J Clin Investig 130:2673–2688
84. Song I et al (2017) Broad TCR repertoire and diverse structural solutions for recognition of an immunodominant CD8(+) T cell epitope. Nat Struct Mol Biol 24:395–406
85. Afonine PV et al (2012) Towards automated crystallographic structure refinement with phenix.refine. Acta Crystallogr Sect D 68:352–367
86. Emsley P, Lohkamp B, Scott WG, Cowtan K (2010) Features and development of Coot. Acta Crystallogr D 66:486–501
87. Pymol The PyMOL Molecular Graphics System, Version 2.0 Schrödinger, LLC
88. Aragao D et al (2018) MX2: a high-flux undulator microfocus beamline serving both the chemical and macromolecular crystallography communities at the Australian Synchrotron. J Synchrotron Radiat 25:885–891

Figures

Figure 1

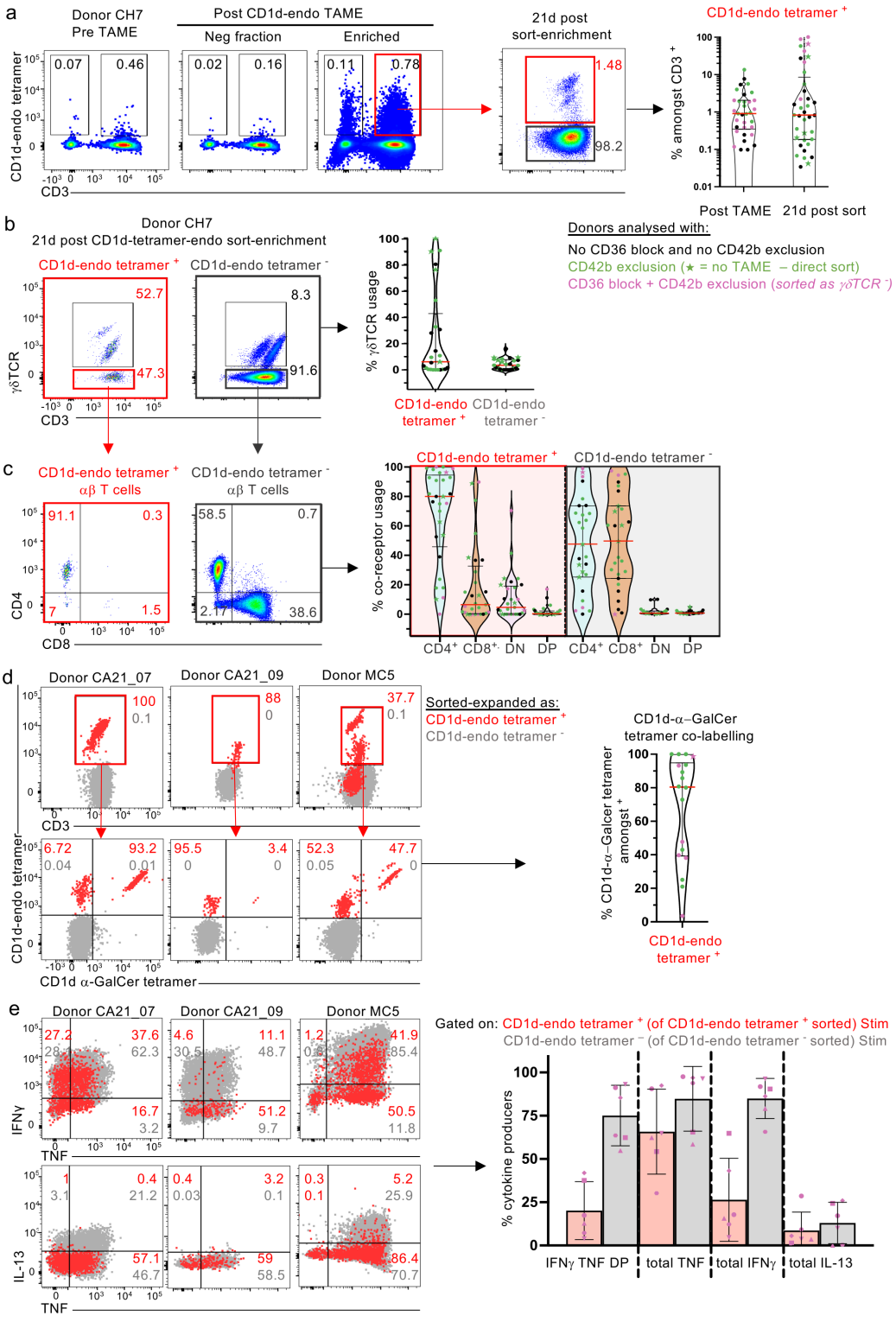


Figure 1

Identification of CD1d-endo-reactive T cells in PBMCs. (**a**) Representative flow cytometry plots showing pre- and post-CD1d-endo tetramer associated magnetic enrichment (TAME), gated on 7AAD$^-$CD14$^-$CD19$^-$CD42b$^-$ single lymphocytes. CD1d-endo tetramer$^+$ CD3$^+$ cells (red gate) were sorted and expanded *in vitro* with plate bound anti-CD3 and anti-CD28 in the presence of IL-2, IL-7 and IL-15. After 21 days, samples were reassessed for their ability to bind CD1d-endo tetramers. Violin plots depict median +/- interquartile range (IQR) of CD1d-endo tetramer$^+$ within CD3$^+$ cells, and each symbol represents an individual donor (33 over 20 experiments for post-TAME, 37 over 21 experiments for 21 days post sort-expansion), coloured according to whether CD36 block was performed prior to CD1d-tetramer staining and/or CD42b$^+$ cells excluded. Stars represent donors (9 over 3 experiments) where no TAME was performed prior to sorting and expansion. After *in vitro* expansion, both CD1d-endo tetramer$^+$ (red) or CD1d-endo-tetramer$^-$ (dark grey) populations were assessed for expression of gδ TCR (**b,** *n*=25 donors), and CD4 or CD8 within the gδ TCR$^-$ ab T cell compartment (**c,** *n*=29 donors), with data summarised in

the violin plots, as per (a). (**d**) Representative overlay dot plots from 3 donors show CD3 *versus* CD1d-endo tetramer (top) or CD1d-endo tetramer *versus* CD1d-a-GalCer tetramer co-labelling (bottom) in cells that had expanded for 21 days after being sorted as CD1d-endo tetramer^{+} CD3^{+} (red) or CD1d-endo tetramer^{-} CD3^{+} (grey underlay). Violin plot shows median +/- IQR of CD1d-a-GalCer tetramer^{+} co-labelling of CD1d-endo tetramer^{+} expanded cells (18 donors over 14 experiments). (**e**) Overlay dot plots show TNF *versus* IFNg or IL-13 intracellular staining on stimulated CD1d-endo tetramer $^{+}$ cells (in red) or CD1d-endo tetramer $^{-}$ (grey) sorted cells that had been expanded *in vitro* for 21 days. Quadrant placement was based on unstimulated controls (21 days post-sort and expansion *in vitro*). Bar graphs summarise cytokine production percentages +/- 95% confidence intervals from 6 donors across 4 experiments. The symbols in graphs shown in (**b-e**) are coded as per (**a**).

Figure 2

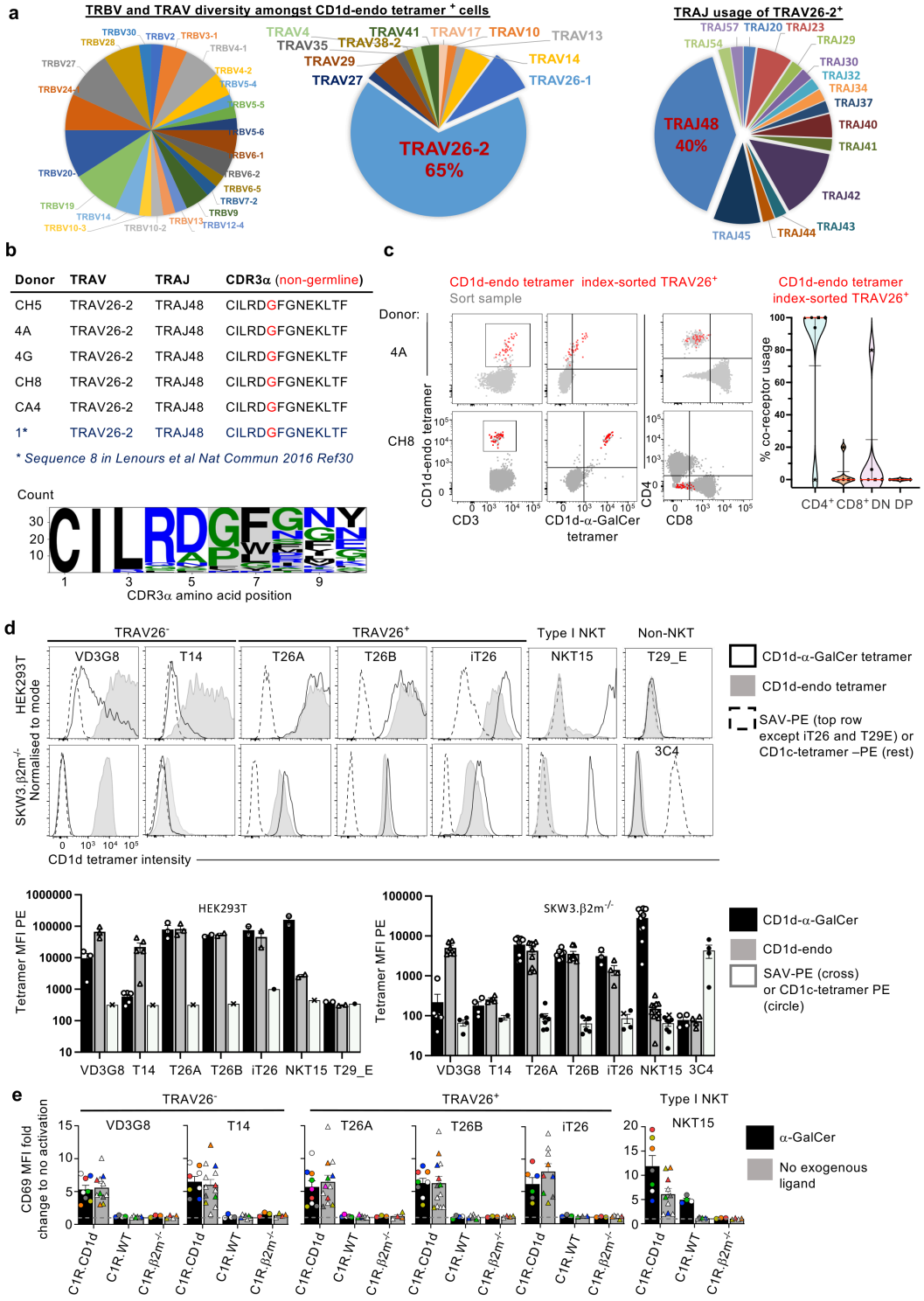


Figure 2

TCR usage amongst CD1d-endo tetramer$^+$ T cells. CD1d-endo tetramer$^+$ T cells were single-cell index-sorted by flow cytometry and TCR sequences determined by nested PCR. (**a**) Pie charts showing *TRAV and TRBV* gene segment diversity, and *TRAJ* gene usage amongst TRAV26$^+$ cells derived from 14 donors over 7 experiments. (**b**) Invariant TRAV26-2-TRAJ48 rearrangement identification across different donors, and sequence conservation of the CDR3α from *n=39* TRAV26-2 clones. Hydrophobic (green) and charged (blue) residues are shown alongside the most common positions for non-germline encoded residues (grey highlight). (c) Representative overlay dot-plots of index-sorted TRAV26$^+$ (red) and total T cells post-culture (grey). Violin plot summarises the CD4/CD8% distribution with median +/- interquartile-range (IQR) of TRAV26$^+$ cells index-sorted from 6 donors over 5 experiments. Five distinct TCR sequences (from **Table 1**) were used to generate transiently transfected HEK293T cells (top) or TCR-transduced SKW3.β2m$^{-/-}$ clones (bottom). (**d**) Representative dot plots showing CD1d-endo and CD1d-α-GalCer tetramer staining of TRAV26$^+$, and TRAV26$^-$ clones. Type I NKT TCR$^+$ clone NKT15 and non CD1d-reactive TCRs (T29_E-top/3C4-bottom) were included as controls. Bar graphs summarise CD1d-tetramer mean fluorescence intensity (MFI) for: HEK293T-transfections (left), from *n*=3 (VD3G8), *n*=5 (T14), *n*=3 (T26A) and *n*=2 (T26B/iT26/NKT15/T29_E) independent experiments; or SKW3.b2m$^{-/-}$ (right), from *n*=6 (VD3G8), *n*=4 (T14/iT26, with *n*=3 for CD1d-a-GalCer), *n*=9 (T26A, *n*=8 for CD1d-a-GalCer), *n*=7 (T26B, with *n*=6 for CD1d-a-GalCer), and *n*=3 (3C4), independent experiments. For *n*=1 HEK293T experiments staining controls included unconjugated SAV-PE (crosses) or CD1c tetramer-PE (spheres). For SKW3.b2m$^{-/-}$ experiments, CD1c tetramer-PE controls were included in *n*=4 (VD3G8) *n*=2 (T14) *n*=6 (T26A) *n*=5 (T26B) *n*=3 (iT26) *n*=6 (NKT15) *n*=4 (3C4) experiments, or SAV-PE for *n*=1 (T26A/T26B/iT26/NKT15). (**e**) TCR-transduced cell lines were co-cultured with wild type C1R cells (C1R.WT) or CD1d transduced (C1R.CD1d), as well as C1R.β2m$^{-/-}$ cells in the presence or absence of α-GalCer (1mg/mL). Bar graphs show CD69 MFI fold increase +/-SEM relative to SKW3.β2m$^{-/-}$ alone. Each dot represents an independent experiment (with:without a-GalCer, respectively): *n*=8:11 (VD3G8), *n*=8:13 (T14), *n*=9:12 (T26A), *n*=8:13 (T26B), *n*=6:9(iT26), *n*=7:10(NKT15) in C1R.CD1d co-cultures; or *n*=4:6(VD3G8), *n*=5:8(T26A), *n*=3:3 (iT26), *n*=4:7 (T26B/T14/NKT15) in C1R.WT co-cultures; or *n*=3:6 (iT26), *n*=3:4 (T26A/T26B/T14/NKT15) in C1R.β2m$^{-/-}$ co-cultures. Experiments shown in blue/grey/green/pink are from the series of experiments shown in Fig. S3a and those in orange/red/yellow are from Fig. S3b (isotype-control treated C1R.CD1ds, performed alongside C1R.β2m).

Figure 3

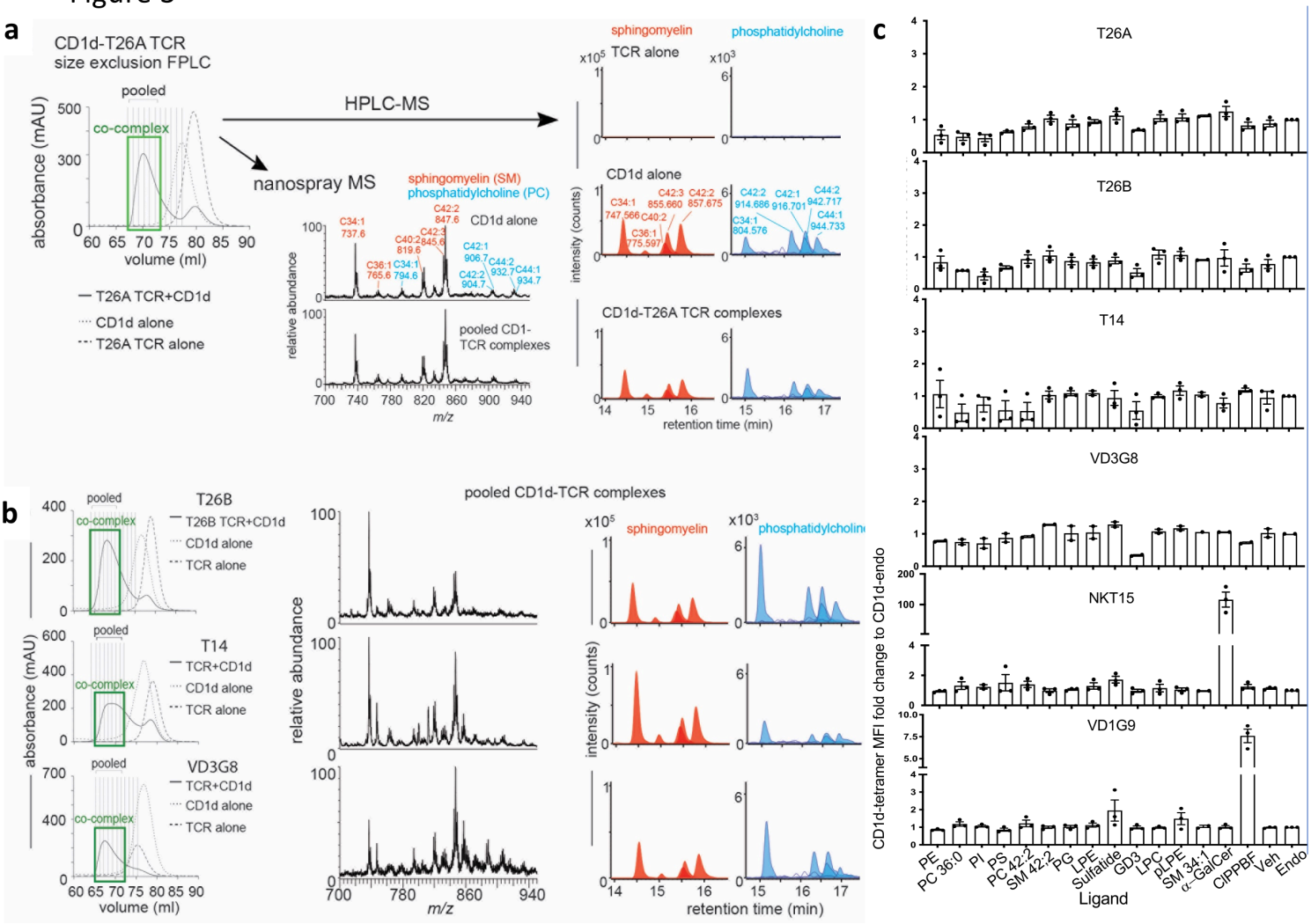


Figure 3

TCR trap determination of T26A TCR-CD1d-endo complexes. (**a**) CD1d alone, T26A TCR alone or CD1d-TCR complexes were introduced to size exclusion chromatography. For CD1d and TCR runs, fractions eluting earlier than monomers (green box) were enriched for CD1d-TCR dimers, as confirmed by

polyacrylamide gel electrophoresis, and were pooled to optimize lipids entering mass spectrometry experiments (MS). Fractions were normalized to protein input and then subjected to lipid elution. The eluents were analysed by the negative mode nano-electrospray (middle) and HPLC–Quadruple Time of Flight–MS (right) to identify ions and mass chromatograms identifiable as SMs (red) and PCs (blue) with the indicated m/z values, total chain length (C) and unsaturations (0, 1, 2). Data is representative of *n=3* independent experiments involving T26A. (**b**) The same analysis for CD1d-T26B, CD1d-T14, and CD1d-VD3G8 TCR complexes was performed for one or two trap experiments, respectively. (**c**) TRAV26^{+} (T26A, T26B) and TRAV26^{-} (T14, VD3G8) CD1d-endo-reactive type II NKT TCR-transduced SKW3.β2m$^{-/-}$ cell lines, were stained with CD1d-tetramers, each exogenously treated with a different ligand. The type I NKT15 TCR and VD1G9 ClPPBF-reactive TCR clones as controls. The fold variation in CD1d tetramer mean fluorescence intensity (MFI) ± SEM, relative to CD1d-endo is shown, from *n=3* independent experiments, each represented by a single point, except for T14 staining with CD1d-LPE, NKT15 with CD1d-PI, VD3G8 stains with all CD1d-tetramers or conditions involving CD1d-SM24:1 where *n*=2.

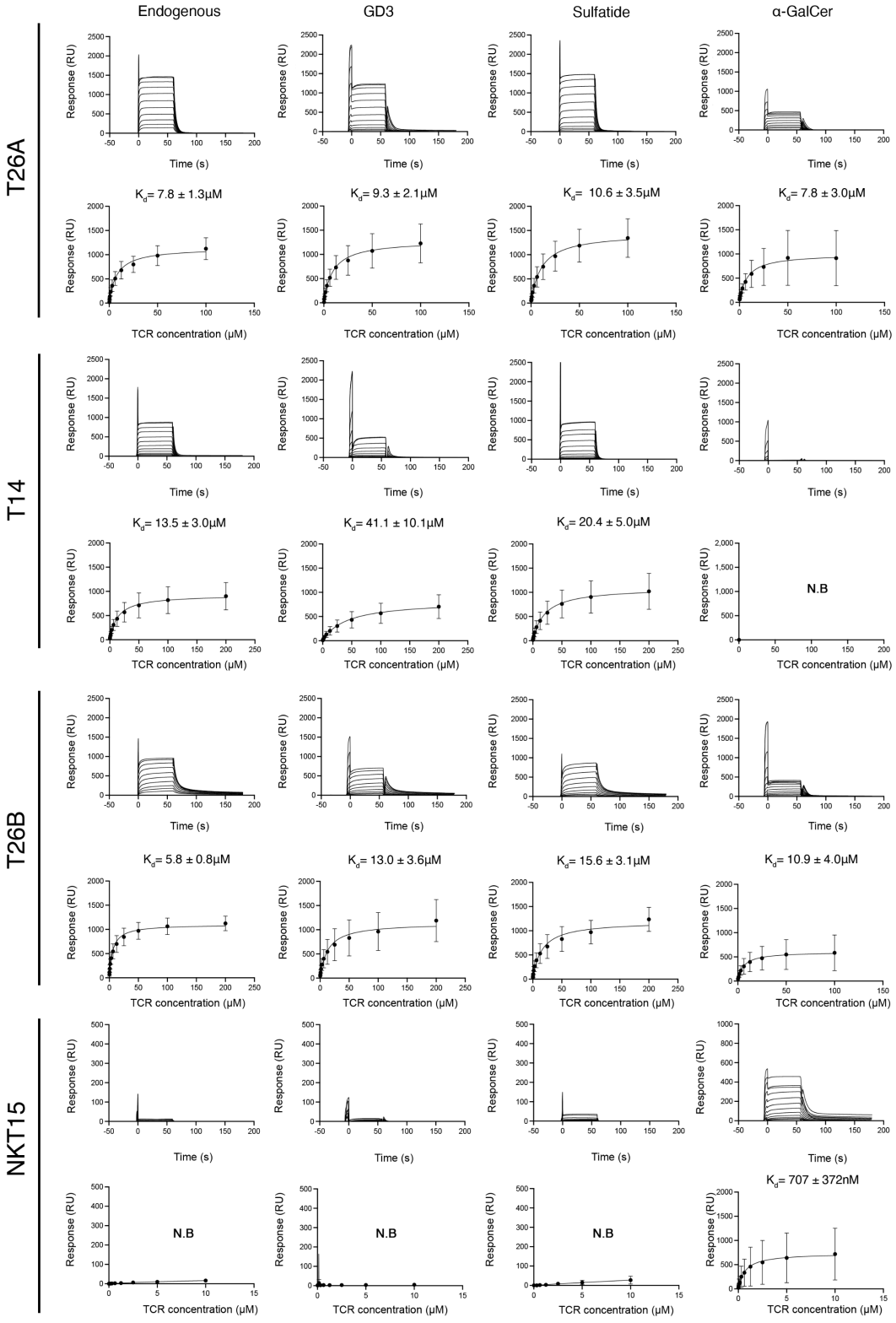


Figure 4

Affinity measurements of type II NKT TCRs. Surface plasmon resonance (SPR) of soluble T14, T26A, T26B and NKT15 NKT TCRs against CD1d-endo, CD1d-GD3, CD1d-sulfatide and CD1d-α-GalCer. The shown sensograms are representative of one experiment performed in duplicate. The resulting Kd ± SEM values are derived from *n=6*independent experiments (T26A, T26B and T14 TCRs) and *n=3* (NKT15 TCR) and each performed in duplicate.

Figure 5

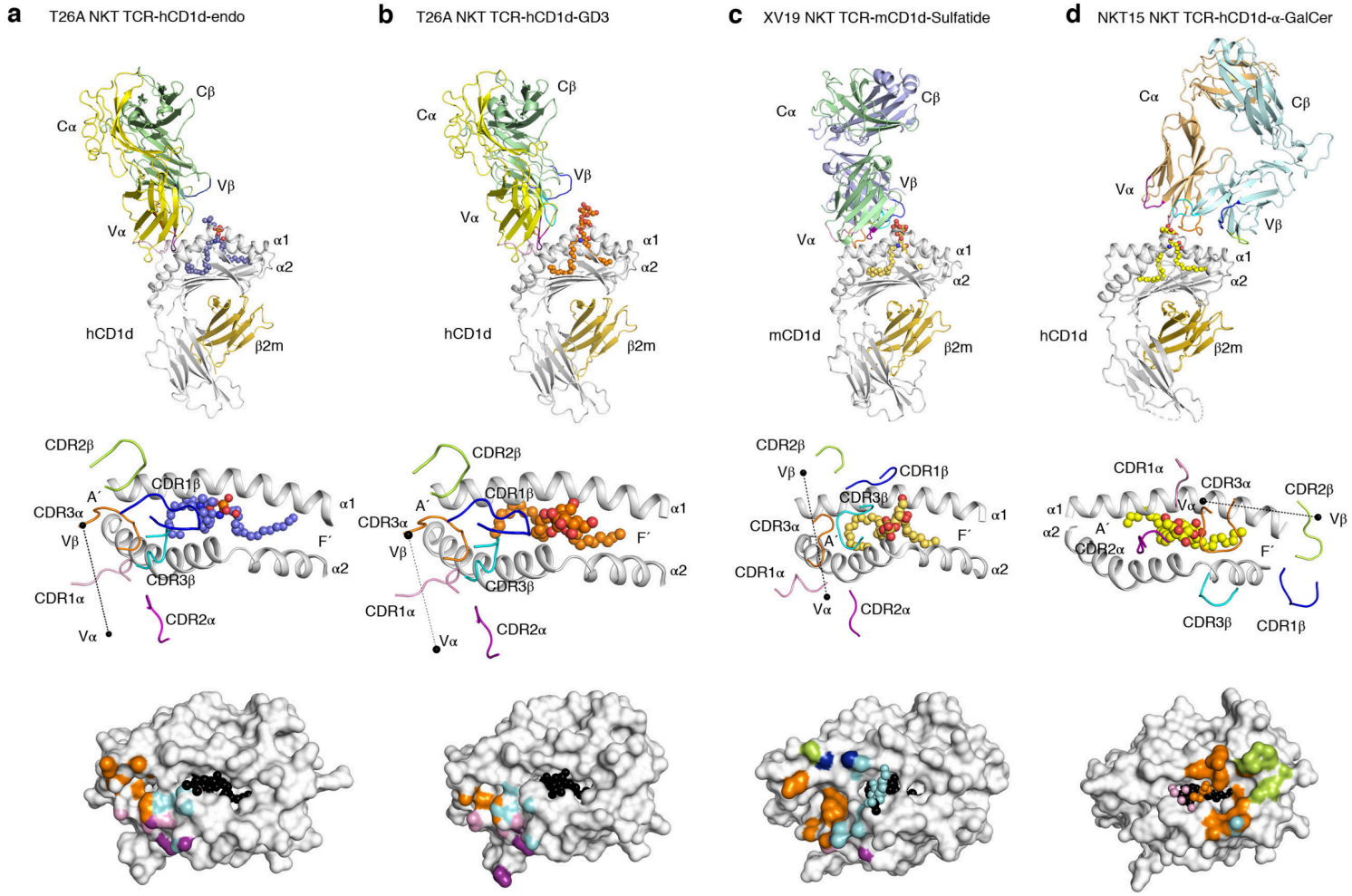


Figure 5

Overview of the mouse type II XV19, human type II T26A and human type I NKT15 NKT TCRs-CD1d ternary complexes. Crystal structure of the (**a**) human T26A TCR-CD1d-endo (SM C40:2 modelled), (**b**) T26A TCR-CD1d-GD3, (**c**) mouse XV19 TCR-CD1d-α-GalCer (PDB code: 4EI5) and (**d**) human NKT15 TCR-CD1d-α-GalCer (PDB code: 2PO6) ternary complexes. The top panels show a cartoon representation of each ternary complex, middle panels depict a top view of the CD1d-binding cleft and the bottom panels illustrate the TCR footprints on the CD1d-lipid molecular surface. Top panels: the CD1d and β2-microglobulin (β2m) molecules are coloured in grey and gold, respectively. XV19 TCRα, light green; XV19 TCRβ, light purple; T26A TCRα, yellow; T26A TCRβ, green; NKT15 TCRα, light brown; NKT15 TCRβ, light blue. The CDR loops are coloured as follows: CDR1α, pink; CDR2α, magenta; CDR3α, orange; CDR1β, blue; CDR2β, lemon green; CDR3β, cyan. The carbon atoms of the lipids, sphingomyelin (SM 40:2), GD3, sulfatide and α-GalCer are coloured violet, orange, pale yellow and yellow spheres, respectively. The oxygen and nitrogen atoms are coloured red and blue, respectively. Middle panels: the lipids are shown as spheres and coloured as in top panels. The center of mass of the respective TRAV and TRBV variable domains are shown as black spheres. Bottom panels: the molecular surface of CD1d is coloured in light grey. Lipids are in black. CDRs TCR contact sites are coloured as in top panels.

Figure 6

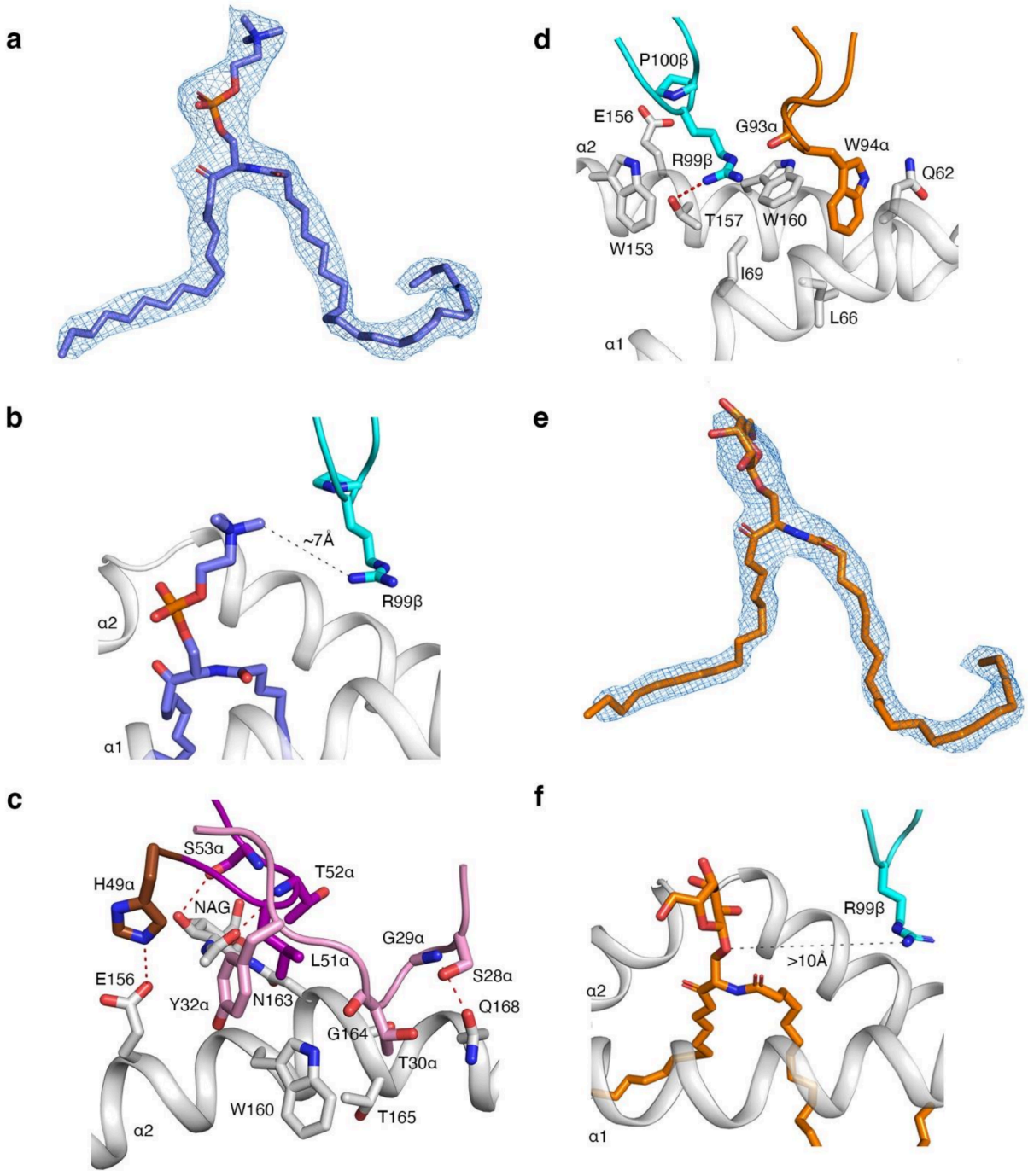


Figure 6

Molecular interactions at the T26A TCR/CD1d-SM. (**a**) 2Fo-Fc electron density map of SM contoured at 0.8σ level. SM is shown as blue sticks. (**b-d**) Molecular interactions of the T26A CDR1α (pink), CDR2α (purple), CDR3α (orange), CDR3β (cyan) and FWα (brown) with CD1d-SM. (**e**) 2Fo-Fc electron density map of GD3 (partially modelled) contoured at 0.8σ level with GD3 shown as orange sticks. (**f**) Molecular interactions of T26A TCR with GD3. For clarity, the α1- and α2-helices of CD1d are shown as cartoon representation and coloured in light grey.

Figure 7

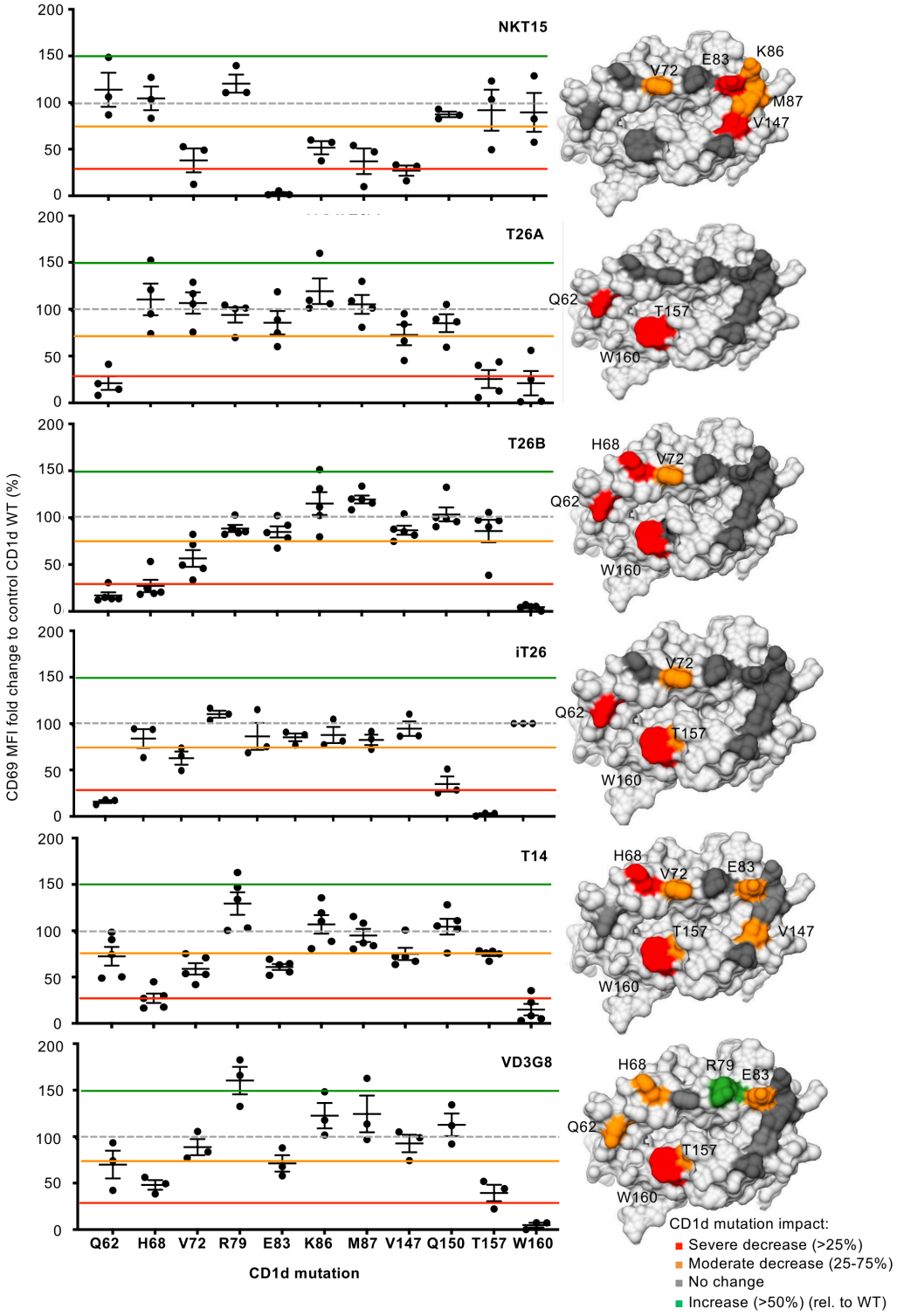


Figure 7

CD1d docking modes of CD1d-endo reactive type II NKT cells. TRAV26^{+} (T26A, T26B and iT26), and TRAV26^{-} (T14 and VD3G8) CD1d-endo reactive NKT TCR-transduced SKW3.β2m$^{-/-}$ cell lines were co-cultured for 16 h with C1R cells each transduced with a single (Ala) mutated version of CD1d. The responses by the type I NKT15 TCR-expressing cell line were analysed as a control. The level of activation (CD69-fold change in comparison to TCR-transduced cell lines alone) elicited by each mutant line is normalized to the response elicited to *wild type* (WT) C1R.CD1d. Data depict mean ± SEM from *n*=3 independent experiments for NKT15, T26A and iT26, *n*=4 for T26A, T26B and *n*=5 for T14. Corresponding CD1d molecular surface maps (Protein Data Bank code: LZT4) are shown to the right of each graph, depicting residues that, when mutated, had no effect (dark grey), a minor (<25%, red), major (<75%, orange) fold decrease, or a fold increase (>50%, green) in CD69 MFI relative to WT CD1d.

Supplementary Files

This is a list of supplementary files associated with this preprint. Click to download.

- PoaandHarpurSupplementaryinformation.pdf